Faraday Discussions

Cite this: *Faraday Discuss.*, 2026, **263**, 9

PAPER

Spiers Memorial Lecture: organic, physical & polymer aspects pivotal in lignin valorization

Nicolò Pajer, [ab] Claudia Crestini [ab] and Dimitris S. Argyropoulos [*c]

Received 4th August 2025, Accepted 21st August 2025
DOI: 10.1039/d5fd00108k

This article addresses current challenges in lignin chemistry by exploring four thematic areas. We begin by examining the major chemical transformations that occur in lignin and discuss the emerging structural understanding of technical lignins. The discussion then shifts to lignin fractionation strategies, which are essential for reducing its inherent heterogeneity and complexity, thereby enabling its use in practical applications. Next, we delve into the chemical and physical behavior of lignin in solution, with particular emphasis on its self-assembly processes relevant to nanoparticle formation. The supramolecular interactions driving these assemblies – such as π–π stacking, hydrogen bonding, and solvent polarity – are analyzed to identify key parameters for designing lignin-based nanomaterials. These materials show promising applications across sectors including agriculture, packaging, cosmetics, and pharmaceuticals. We then consider the broader valorization of lignin, focusing on the rheological and antioxidant properties of lignin fractions. Particular attention is given to their role in forming polymer blends with polyethylene, highlighting their influence on thermal stability and mechanical performance. Finally, we explore lignin's potential as a non-petroleum precursor for carbon fiber production. We critically assess the main barriers in this field, such as lignin's relatively low molecular weight and thermal behavior, which hinder effective fiber formation and graphitization. Strategies to address these challenges, including the integration of fractionation techniques with chemical modifications, are discussed. The article concludes with a review of recent efforts to overcome the limitations of lignin graphitization and enhance its viability as a sustainable carbon fiber source.

1. Introduction

Contemporary socio-economic pressures demand the implementation of green technologies to confront global challenges such as climate change and the

[a]*Department of Molecular Sciences and Nanosystems, Ca' Foscari University of Venice, Via Torino 155, 30170 Venezia – Mestre, Italy*
[b]*CSGI – Center for Colloid and Surface Science, Via della Lastruccia 3, 50019 Sesto Fiorentino, Italy*
[c]*Departments of Chemistry & Forest Biomaterials, North Carolina State University, 2820 Faucette Dr, 27695 Raleigh, North Carolina, USA. E-mail: dsargyro@ncsu.edu*

dwindling availability of fossil fuels. This shift underscores the need to utilize renewable feedstocks – particularly lignocellulosic biomass – for the production of high-value chemicals traditionally derived from petroleum sources. While the industrial conversion of biomass's carbohydrate components – cellulose and hemicelluloses, which constitute 65–70% of its mass – is well established, enabling the synthesis of platform chemicals like furfural, hydroxymethylfurfural (HMF), and related compounds, the efficient utilization of lignin, which comprises the remaining 30–35%, continues to pose significant challenges. These challenges primarily stem from lignin's structural complexity, resistance to chemical modification, and inherent heterogeneity.

Lignin (Fig. 1), the most abundant renewable aromatic biopolymer, is synthesized through the end wise random polymerization of enzymatically generated phenoxy radicals of mainly three monolignols: *p*-coumaryl, coniferyl, and sinapyl alcohol. This process yields an irregular macromolecule, lacking the defined primary structure typical of other biopolymers like cellulose, proteins, or nucleic acids. The monolignol units are interconnected *via* a variety of chemical bonds, including ether bonds, carbon–carbon linkages, and mixed ether–carbon–carbon linkages.[1] Among the ether linkages, β-O-4′ arylglycerol ether and 4-O-5′ diaryl ether are the most prevalent. Key carbon–carbon bonds include the 5–5′ biphenyl linkage, while mixed linkages are represented by structures such as phenylcoumaran (β-5′) and resinol (β–β′). Additionally, lignin contains various functional groups – methoxy, hydroxyl, carbonyl, olefinic, and ester moieties – whose distribution is influenced by factors such as plant species, geographical origin, and most notably, the extraction method employed.[2–4]

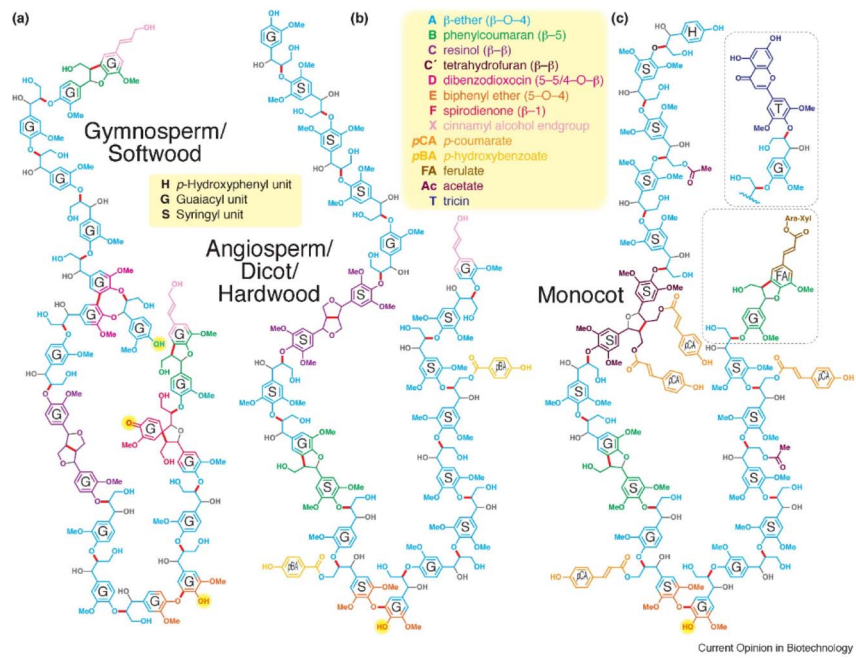

Fig. 1 Current lignin structure according to Ralph, Lapierre, and Boerjan.[4] Reproduced from ref. 4 with permission from Elsevier, copyright 2019.

The valorisation of lignin constitutes a broad and dynamic field, beginning with the sourcing of raw materials. Traditional strategies focus on technical lignins, obtained as by-products of pulping processes and biorefineries. More recently, the lignin-first approach has emerged, Kraft lignin, a by-product of the production of pulp, is currently incinerated in the recovery boiler during the chemical recovery cycle, generating valuable bioenergy and recycling inorganic chemicals to the pulping process operation. Removing lignin from the black liquor or its gasification lowers the recovery boiler load enabling increased pulp production. During the past ten years, lignin separation technologies have emerged and the interest of the research community in valorizing this underutilized resource has been invigorated. Overall, it is anticipated that this effort will inspire further work for developing and using kraft lignin as a commodity raw material for new applications, undeniably promoting pivotal global sustainability concerns which seek to valorise lignin as a co-product through novel, yet unscaled, biomass processing technologies. In both cases, chemical transformation – whether by polymerisation or depolymerisation – underpins the utilization of lignin. Polymerisation strategies aim to generate high-molecular-weight fractions with tailored functionalities for applications such as adhesives, carbon fibre precursors, and additives for composites. Alternatively, depolymerisation approaches seek to produce low-molecular-weight compounds for applications ranging from biofuels to antioxidants and fine chemicals, often employing oxidative or reductive catalytic pathways.

This effort offers a critical outline of key aspects in lignin valorisation, beginning with an overview of the chemical transformations occurring during extraction under pulping conditions. The role of lignin fractionation as a strategy for producing more homogeneous, application-ready lignin streams is then discussed. Subsequently, the association behavior of lignin and its implications for the fabrication of lignin-based materials is examined, followed by selected aspects of lignin polymer chemistry with emphasis on the effect of lignin fractionation on the rheological behavior and oxidative thermal stability of lignin in polymeric blends. Finally, the challenges associated with the production of carbon fibers from lignin are discussed.

2. Technical lignins differ from native lignins

Technical lignins are the primary by-products of the pulping industry and biorefineries. The sulfate and sulfite processes are the most widely used delignification methods that enable the isolation of lignin as solubilized species in alkaline or acidic aqueous media, respectively. More specifically, for the sulfate (kraft) process, lignin is isolated from the alkaline solutions through precipitation *via* pH reduction, using concentrated inorganic acids (*e.g.* sulfuric acid) and/or carbon dioxide. For the sulfite process, lignin is isolated by concentrating the acidic solutions in boilers, yielding lignin as an encrusting, powdery product. Lignins isolated from both processes are often contaminated with inorganics, such as sodium and/or calcium sulfites, carbonates, and/or sulfide species. These are important salt species used in pulping and are eventually recycled.

Organosolv processes, on the other hand, form the basis of modern biorefineries yielding lignin that is soluble in organic solvents (*e.g.* methanol, ethanol), eventually isolated after solvent evaporation. Since no inorganics are

involved in the organosolv processes, higher purity lignins are obtained compared to those that emerge from conventional pulping liquors.

Technical lignins are named according to the process used for their isolation. Specifically, lignins isolated from sulfate pulping are referred to as "kraft lignins", those from the sulfite process as "lignosulfonates", and those from organosolv processes as "organosolv lignins". A comparison of the structural features – such as functional group content (*e.g.* methoxy and hydroxy groups), bonding pattern distribution (*e.g.* aryl-glycerol-β-aryl ethers), and molecular weight – between technical lignins and native lignins, reveals significant differences, highlighting the strong influence of isolation conditions. Numerous studies have investigated the impact of both conventional pulping (kraft & lignosulfonate) and organosolv conditions on the structure of lignins. In general, both delignification processes involve the degradation of lignin through the cleavage of interunit linkages, which simultaneously introduces hydroxyl or alkoxy groups on the lignin.

By choice, from this point on this effort will be focused on examining the organic, physical & polymer aspects pivotal in kraft lignin valorization, since using kraft lignin as a commodity raw material for new applications undeniably has potential in promoting pivotal global sustainability concerns.

2.1 The chemistry of pulping; an outline

The chemistry of kraft pulping was recently reviewed.[5] The severe conditions of the kraft pulping process originate from a wide array of reactions that profoundly alter the structure of lignin. As such, kraft lignin is substantially modified in comparison to native lignin in wood and to milled wood lignin (MWL) obtained from the same starting material. From this perspective, the term "lignin" may even be considered misleading and would be more accurately defined as a class of compounds sharing aromatic building blocks as a common feature. Consequently, elucidating its structure is a complex undertaking that can only be achieved by combining advanced analytical techniques such as modern nuclear magnetic resonance (NMR), mass spectrometry, size exclusion chromatography *etc.*

Under kraft pulping conditions, lignin undergoes fragmentation and dissolution through a series of reactions, primarily taking place at the aryl-glycerol-β-aryl ether (β-O-4′) linkages.[6–9] However, it appears that several radical redox reactions also occur on the liberated monomeric or oligomeric lignin fragments, leading to recondensation processes in parallel with further fragmentation and reduction reactions along the lignin side chains.

The β-O-4′ is the most common bonding pattern in native lignins. This bond is primarily cleaved by two distinct ionic mechanisms, as illustrated in Fig. 2. One such mechanism, referred to as "slow sulfide independent reaction" occurs predominantly in non-phenolic structures and gives rise to an "*endo*-depolymerisation" process (Fig. 2A).[9,10] This reaction is initiated by the deprotonation of the Cα hydroxy group, followed by an intramolecular nucleophilic substitution that leads to the formation of an epoxide intermediate and subsequent cleavage of the aryl–alkyl ether linkage. The main reaction pathway is a "fast sulfide dependent reaction" (Fig. 2B) that occurs at the phenolic end-units.[7] Under kraft pulping conditions, lignin structures are present in the form of phenolate anions. A key step involves the formation of a quinone methide intermediate, generated

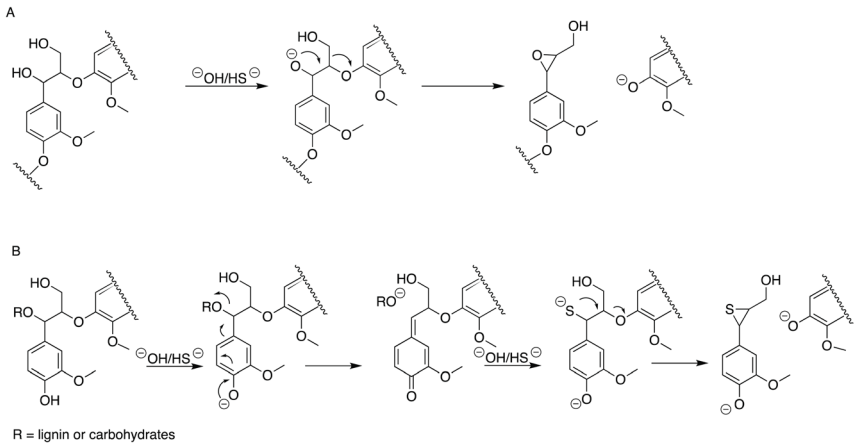

Fig. 2 Cleavage of non-phenolic and phenolic β-O-4 bonds during kraft pulping. (A) Slow sulfur-independent reaction, *endo*-depolymerisation; (B) fast sulfur-dependent reaction, *exo*-depolymerisation.[7,8] Reproduced from ref. 5 with permission from Wiley, copyright 2023.

through the elimination of the Cα hydroxyl group. This quinone methide is then subjected to nucleophilic attack by the highly reactive hydrosulfide anion, followed by an intramolecular nucleophilic substitution that produces an episulfide intermediate. This sequence ultimately leads to the cleavage of the β-O-4′ aryl ether bond, resulting in lignin "*exo*-depolymerisation".[11,12]

A central step in the modification and depolymerisation of lignin during kraft pulping is the formation of a quinone methide intermediate, resulting from the oxidation of phenolic end-groups. This reactive intermediate is then attacked by nucleophilic hydrosulfide ions, leading to the cleavage of β-O-4′ interunit linkages (Fig. 3A). Alternatively, phenolic aryl enol ether end-groups may undergo formaldehyde elimination (Fig. 3B).[13] The generation and chemical behavior of the quinone methide intermediate also influences the fate of other lignin substructures, such as phenylcoumarans (β-5′) and β-1 linkages. In contrast to the cleavage observed in β-O-4′ linkages, quinone methides formed from β-5′ and β-1 units (Fig. 3C) tend to eliminate formaldehyde to produce stilbene-type end groups. However, this transformation does not lead to further depolymerisation of the lignin structure.[12]

Kraft lignin is characterized by a markedly reduced content of aliphatic side chains, with the proportion of oxygenated aliphatic carbons significantly lower than that of aromatic units contrasting with the typical ratios observed in native-like lignin preparations such as milled wood lignin (MWL).[14,15] This indicates that extensive side-chain fragmentation pathways are at play. In particular, cleavage between the C1 and Cα positions take place under alkaline conditions at terminal phenolic sites in the lignin structure, through retro-aldol reactions, resulting in the formation of monomeric phenolic compounds (Fig. 3D).[12,16] Importantly, these monomeric phenols, which lack the original lignin side chains, are still chemically reactive. Moreover, during kraft pulping, both monomeric and polymeric phenols – whether retaining the original or modified aliphatic side chains –

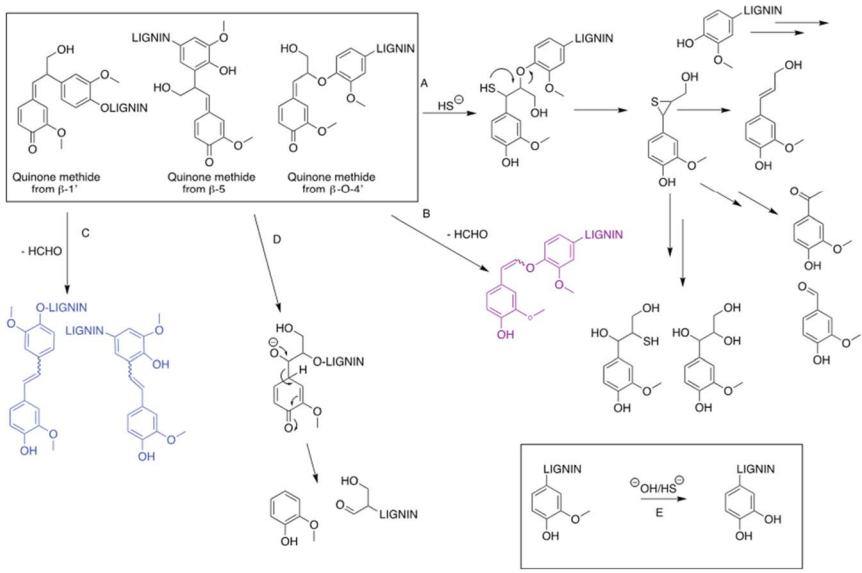

Fig. 3 Key reactions from quinone methide intermediates during kraft pulping. Reproduced from ref. 5 with permission from Wiley, copyright 2023.

undergo substantial demethylation at the C3 position of the aromatic ring. This transformation leads to the formation of catechols, accompanied by the release of methyl mercaptan and dimethyl sulfide (Fig. 3E), the compounds chiefly responsible for the characteristic odour associated with kraft pulp mills.[12,16]

The description so far might indicate that practically all lignin could be removed from the wood by depolymerization as described above. This is not the case in practice, and the main product, the pulp, contains 5–10% lignin. A variety of C–C linkages originally present in the lignin as well as others formed during kraft pulping, together with a significant variety of unsaturated centers, still remain in the residual lignin. To eliminate the final lignin, bleaching is required.[17]

The occurrence of non-oxygenated aliphatic side chains, as well as moieties containing two or a single carbon atom(s), in kraft lignin has been well documented.[16,18,19] However, their precise origin remains unclear and warrants further investigation. One plausible explanation for their formation involves complex radical-based redox reactions taking place during the kraft pulping process. Indeed, in-depth studies of pulping chemistry have revealed the generation of radical sulfur species.[19,20] Comprehensive structural analysis of kraft lignin, isolated from wood that had been pre-extracted with acetone, has clearly demonstrated that the reduced, non-oxygenated aliphatic side chains present in kraft lignin do not originate from residual extractive compounds.[16] This finding suggests the involvement of intricate redox processes, potentially facilitated by sulfur-containing species.

In-depth structural investigations of kraft lignin reveal a significantly higher degree of branching compared to the original lignin present in wood, typically isolated as milled wood lignin (MWL). Early qualitative evidence from permanganate oxidation indicated extensive branching.[21] More recent analyses,

employing quantitative ^{13}C NMR and QQ-HSQC techniques, have estimated the degree of branching in kraft lignin to be approximately 84%.[16] Under the severe conditions of kraft pulping, hydrosulfide gives rise to various sulfur-containing species, including polysulfide, elemental sulfur, thiosulfate, and sulfate.[22] As a result, radical redox reactions play a significant role in shaping the final structure of kraft lignin and must be considered alongside ionic mechanisms.[22–26] The monomeric, oligomeric, and polymeric lignin fragments produced *via* ionic mechanisms during pulping, consequently undergo extensive and complex radical oxidative coupling reactions. This has a profound impact on the structure of the resulting lignin. Such a reaction pathway accounts for the high degree of branching observed in kraft lignins. Fig. 4 presents radical repolymerisation pathways that have been proposed in earlier studies. In addition, a broad range of aliphatic signals can be observed in the HSQC spectra of kraft lignins. These include signals corresponding to aryl-acetic acid, aryl-hydroxy-acetic acid, aryl ethyl ketone, aryl propanol, and aryl hydroxyethyl ketone. It is likely that these aliphatic groups originate from the aforementioned redox processes.[16,20] Indeed, it has been clearly established that they are not attributable to the presence of, or reactions involving, extractable aliphatic compounds naturally occurring in wood.

It is, therefore, readily anticipated that kraft lignins are highly polydisperse polymers. They exhibit relatively low number-average (M_n) and weight-average

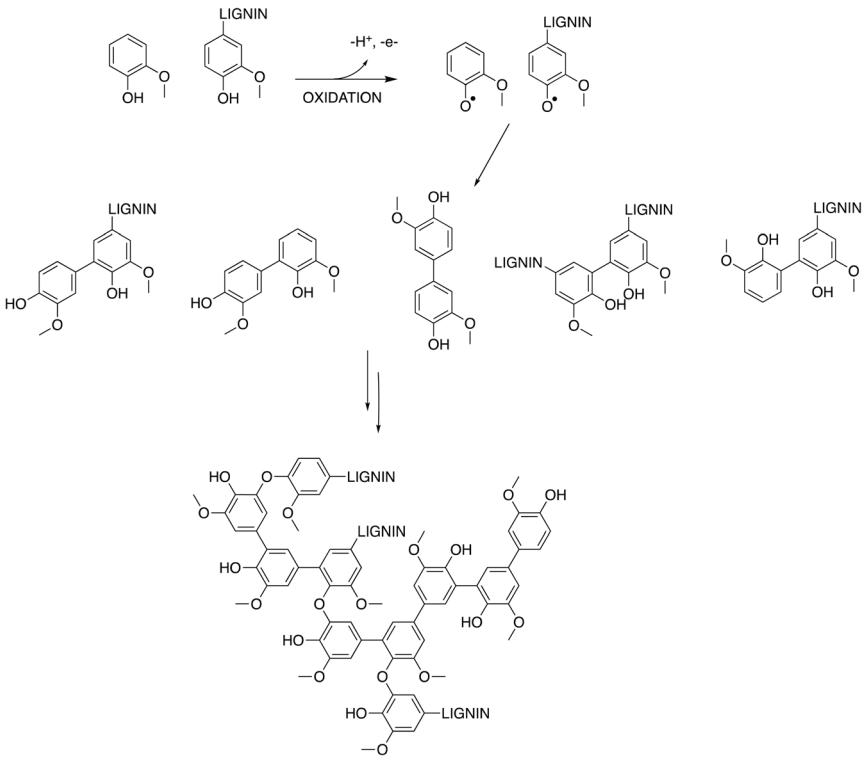

Fig. 4 Possible radical oxidative coupling modes of lignin fragments released during kraft pulping. Reproduced from ref. 16 with permission from the Royal Society of Chemistry, copyright 2017.

Table 1 Molecular weight distribution in softwood and hardwood kraft lignins. Reprinted with permission from ref. 5

Sample	M_n	M_w	Method	Reference
Softwood				
Softwood kraft lignin	1600	3500	Osmometry	28
Softwood kraft lignin	1710	2570	Maldi-TOF	29
Softwood kraft lignin	1820	3100	GPC	29
Indulin AT	1200	2990	Maldi-TOF	29
Indulin AT	1340	3400	GPC	29
Softwood kraft lignin	1400	6000	GPC	16 and 30
Hardwood				
European beech kraft lignin	1044	1711	GPC	31
Eucaliptus kraft lignin	1273	4200	HPLC	32
Eucaliptus grandis kraft lignin	910	1740	GPC	33
Hardwood kraft lignin	1000	3900	HPLC	34
Hardwood kraft lignin	1000	3300	HPLC	34
Indulin hardwood	1300	2700	GPC	35
Hardwood kraft lignin	1263	2400	GPC	36
Hardwood kraft lignin	1793	3290	GPC	37

(M_w) molecular weights, with M_n values ranging from 800 to 2000 and M_w values between 1700 and 6000, as detailed in Table 1. These findings indicate that a significant proportion of kraft lignins possess a molecular mass of approximately 800 daltons, corresponding to a degree of polymerisation in the range 1 to 6.[27]

The introduction of a fractional precipitation method by Argyropoulos and his team has made it possible to isolate kraft lignin samples with a high degree of uniformity in terms of molecular weight, functional group composition, and quantity.[38,39] This advancement has opened up a new avenue for the structural investigation of kraft lignin. Using this technique, both acetone-soluble and acetone-insoluble fractions were obtained, along with several soluble fractions exhibiting distinct molecular weight distributions. These fractions were subjected for detailed structural analyses employing ^{31}P NMR, ^{13}C NMR, quantitative HSQC (QQ-HSQC), and gel permeation chromatography (GPC). The outcome of this extensive study led to the proposal of a revised structural model for kraft lignin.[16]

According to the new model, kraft lignin is composed of a high molecular weight acetone-insoluble fraction and a lower molecular weight acetone-soluble component. The insoluble fraction retains structural features reminiscent of native lignin in wood, albeit with significant alterations. It is more extensively branched and features heavily modified side chains. Specifically, it contains stilbene and aryl enol ether motifs, while classical lignin units such as β-O-4 linkages, phenylcoumarans, and pinoresinols are largely absent. The aliphatic side chains are often reduced or cleaved. This structural profile is believed to result from reactions occurring during kraft pulping, particularly complex redox-driven side-chain reductions and fragmentations.

In contrast, the acetone-soluble fraction is characterized by a highly branched polyphenolic structure with a marked depletion of the oxygenated side chains typically associated with lignin. It contains a higher concentration of phenolic

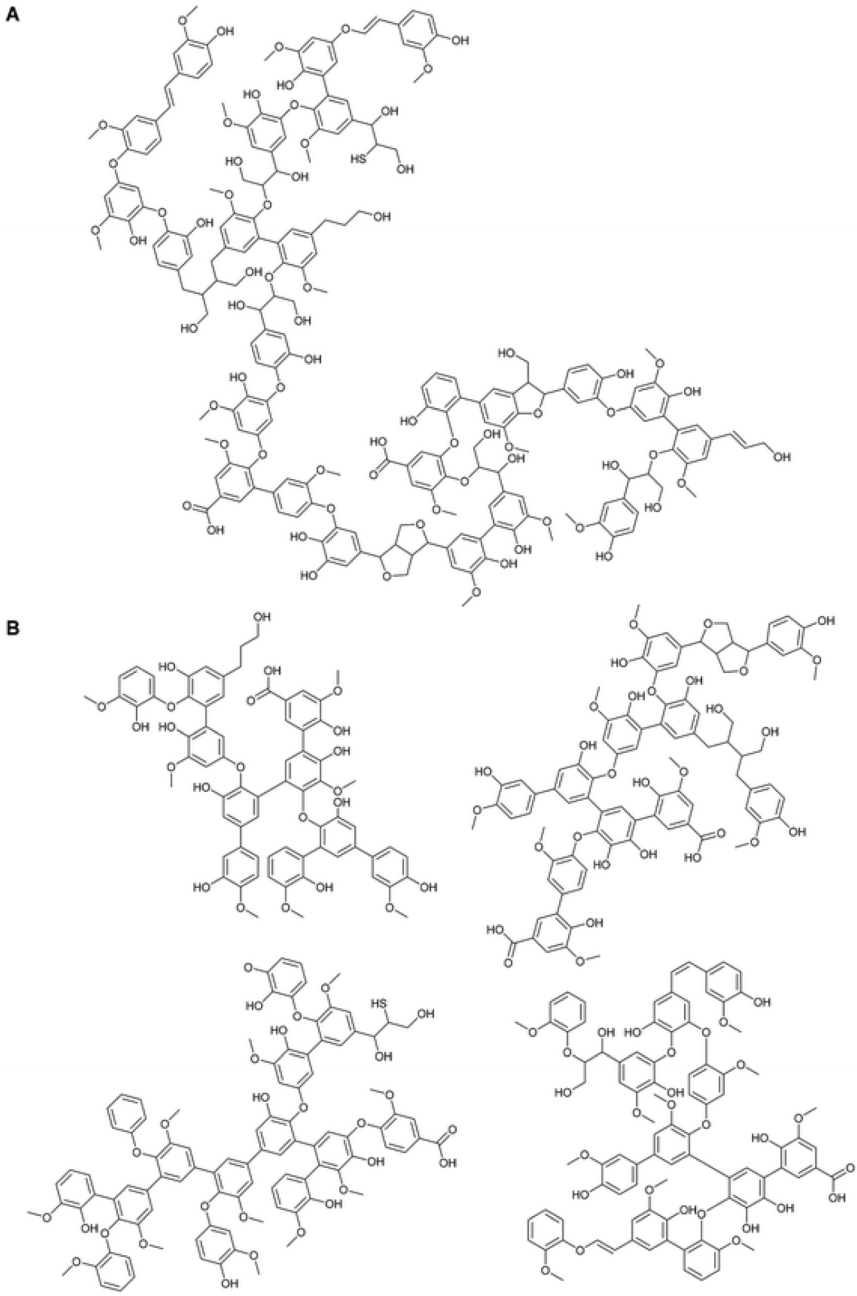

Fig. 5 Proposed new structure for softwood kraft lignin (SKL) composed of a mixture of: (A) large lignin segments containing some native lignin structures; (B) smaller lignin segments enriched with phenolic character. Reproduced from ref. 16 with permission from the Royal Society of Chemistry, copyright 2017.

hydroxyl groups compared to the insoluble fraction. This material is likely formed through extensive oxidative coupling of monomeric phenolic intermediates liberated during the pulping process, as illustrated in Fig. 3. The proposed

structural representation of softwood kraft lignin (SKL),[16] which takes into account the relative abundances of functional groups and the extent of branching, is presented in Fig. 5.

3. Lignin valorisation & fractionation processes

A key challenge in lignin valorisation resides in its conversion into consistent, valuable materials with defined molecular weight and properties. This can be achieved either *via* chemical derivatisation – using stoichiometric or catalytic processes – or through fractionation, which involves separating lignin into fractions with specific characteristics. The heterogeneity of lignin, stemming from both its biogenesis and the uncontrolled transformations during extraction, complicates fractionation. Molecular weight, functional groups, and bonding patterns are all interdependent and influence solubility and polarity, making it difficult to isolate consistent fractions. Therefore, a thorough structural analysis of each fraction is essential. This necessity, first recognized by Argyropoulos and his team,[38] laid the foundation for ongoing research into effective lignin fractionation and valorization.

As reviewed by Gigli and Crestini,[39] fractionation strategies can be broadly divided into two main categories: (a) solvent-based fractionation and (b) membrane-mediated fractionation. Among these, solvent-based methods are more commonly employed due to their simpler and more scalable operations, requiring less stringent conditions than the costly ultra- and nano-filtration steps involving polymeric or ceramic membranes.

Solvent fractionation strategies can, in turn, be classified into three main categories: fractional precipitation, pH-dependent precipitation, and solvent extraction.

3.1 Fractional precipitation

A rigorous example of lignin fractionation *via* fractional precipitation was reported by Cui *et al.*[38] This method involves dispersing lignin in a suitable solvent, producing a soluble fraction and an insoluble one, the latter of which can be directly isolated *via* filtration. Additional fractions are obtained by gradually adding an anti-solvent to the soluble portion, altering the polarity of the solution. As the anti-solvent content increases, fractions with distinct structural features precipitate. In the work of Cui with SKL – the most common technical lignin – partitioning with acetone at room temperature yielded an acetone-soluble fraction (ASKL) and an acetone-insoluble fraction (AIKL). Further addition of hexane to the acetone ASKL solution enhanced the solvent hydrophobicity and led to the isolation of subsequent fractions. Starting from ASKL, which had a broad dispersity of 4.7 and a weight-average molecular weight of approximately 13 000 Da, the resulting fractions had narrower dispersions (1.1–2.5) and molecular weights ranging from 1500 to 5900 Da (Fig. 6).

Notably, the weight-average molecular weights of these fractions were linearly correlated with the aliphatic-to-phenolic hydroxyl group ratio, indicating that fractional precipitation is governed by both molecular weight and hydroxyl content. A comprehensive study by Crestini applied 1D and 2D NMR to acetone-fractionated SKL, finding the acetone-soluble fraction to have a lower molecular

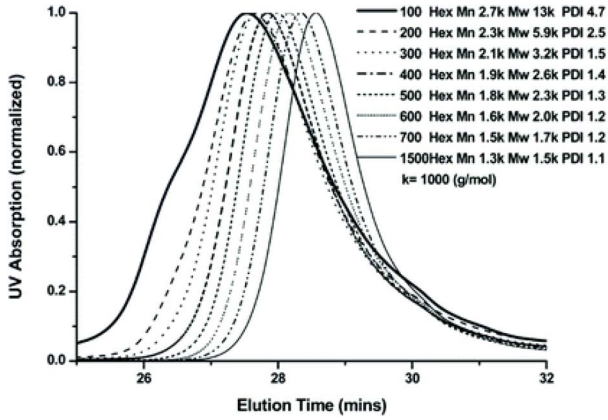

Fig. 6 Size-exclusion chromatograms of SKL fractions isolated *via* fractional precipitation. Reproduced from ref. 38 with permission from the American Chemical Society, copyright 2014.

weight and a higher condensation degree, suggesting its origin in radical re-polymerisation. The acetone-insoluble fraction retained more native lignin features and a higher aliphatic hydroxyl content.[40] This method was proven reliable across lignins of various origins and pulping methods. Subsequent to the early fractionation work of the Argyropoulos group, various researchers embarked on also offering alternative solvent systems – such as acetone, methanol, ethanol, ethyl acetate, tetrahydrofuran, γ-valerolactone, and water.[41–44] The fractional precipitation method can be considered as the state of the art since it produces a continuum of narrowly dispersed lignin fractions with a predictable functional group content.[38]

3.2 pH-dependent precipitation

Offers an alternative by-passing the initial lignin isolation by directly treating black liquors. Upon acidification under controlled conditions, lignin fractions precipitate. While differences in molecular weight or hydroxyl content between fractions obtained at varying pH levels are not relevant, a significant increase in purity – especially a reduction in polysaccharide contamination – is observed when pH is lowered below 2. In contrast, higher pH precipitates tend to contain more hemicellulose impurities.[45–47]

3.3 Solvent extraction

Exploits differences in solubility among lignin fractions. This approach is influenced by the hydrogen bonding ability of lignin and the Hildebrand parameter of the solvent.[48] Due to its simplicity, it is particularly valuable for industrial scaling up. The process involves dispersing lignin in a selected solvent under stirring at room temperature, followed by centrifugation or filtration to isolate the soluble fraction. Repeated extractions using fresh solvent ensure thorough fractionation, with final recovery achieved *via* vacuum evaporation. For low-boiling solvents like acetone, continuous solid–liquid extractors of the Soxhlet-type have been effectively applied.[49,50]

Compared to pH-dependent methods, solvent extraction not only allows customization of purity but also of structural properties such as functional group content, bonding pattern, and molecular weight. For instance, Saito demonstrated that using different solvents (methyl ethyl ketone (MEK), methanol (MeOH), and tetrahydrofuran (THF)) was possible to isolate fractions characterized by different features.[51] THF yielded a soluble fraction with the highest yield (~60%), while MEK yielded the lowest (~20%), with MeOH yielding intermediate values. Soluble fractions consistently showed lower molecular weights and narrower dispersion (1.5–1.8) than insoluble ones. Notably, THF-soluble fractions had an average molecular weight of 1360 Da, MeOH-soluble fraction 1610 Da, and MEK-fraction 1100 Da. Soluble fractions also showed a lower content of aliphatic hydroxyl groups than insoluble ones – most markedly in the case of MEK (0.39 mmol g^{-1} *vs.* 0.63 mmol g^{-1}). A correlation was clear between solvent polarity and phenolic hydroxyl group content, with MeOH yielding the highest value (0.70 mmol g^{-1}). Thermogravimetric analyses revealed lower thermal stability of soluble fractions, and a linear relationship between molecular weight and char yield, suggesting criteria for carbon fibre precursors.

An investigation into Hildebrand theory employed acetone/water mixtures.[52] Solubility increased (over 80%) with water solution containing acetone above the 50%, but correlation with Hildebrand values was inconsistent. Soluble fractions consistently showed lower aliphatic-to-phenolic hydroxyl group ratios and syringyl-to-guaiacyl ratios compared to the original lignin, with decreasing values as the polarity of the solvent employed increased.

An improved modification of solvent fractionation is sequential solvent extraction, where a series of solvents (hexane, methanol, acetone, dioxane, *etc.*) is used (Fig. 7).[46,49,50,53]

Higher molecular weight fractions generally show more aryl-glycerol-β-aryl ether linkages and aryl ether bonds,[54–56] while lower fractions have more hydroxyl groups and saturated aliphatic chains.[53,55,56] Thermal stability and glass transition temperature correlate positively with molecular weight.[46,50,53] Findings regarding syringyl-to-guaiacyl ratios remain inconsistent – some show positive correlation

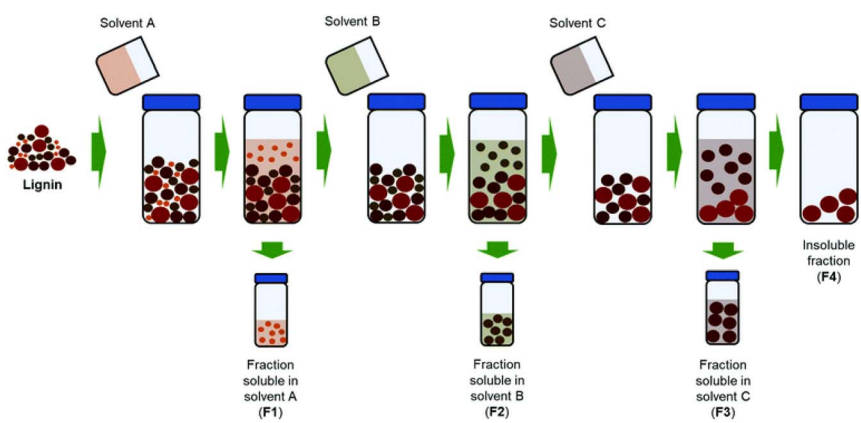

Fig. 7 Sequential solvent extraction. Reproduced from ref. 39 with permission from the Royal Society of Chemistry, copyright 2020.

with molecular weight,[50] others report the opposite or no change.[54,57] Sequential extraction using both aprotic (*e.g.*, acetone) and protic solvents (*e.g.*, methanol) also isolates lignin–carbohydrate complexes (LCCs).[49] More advanced methods use DMSO/*t*-butylammonium hydroxide systems and barium hydroxide to separate by precipitation LCCs, by polysaccharide type (glucomannan, xylan, or glucan),[58–60] with clear differences in branching, unit composition, and functional groups.[59] In corn stalk lignin, ethanol–water systems revealed that higher water content led to fractions with higher molecular weight, greater thermal stability, more guaiacyl units, and fewer phenolic acids.[61] Sustainable alternatives, for instance using glycerol–ethanol mixtures, also demonstrated effective separation by molecular weight and guaiacyl content.[57]

Despite intrinsic limitations such as fouling and membrane lifespan, membrane fractionation offers isolation of lignin fractions with narrow molecular weight distributions and specific physico-chemical properties.[62] Ultrafiltration, first applied in the 1970s to technical lignin and lignosulfonates,[63] is typically performed under low to medium pressure. Early membranes included polyamide and cellulose acetate, while more recent studies have utilised polysulfone and polyether sulfone films. Smaller membrane cut-offs reduce dispersity and increase phenolic hydroxyl content.[64] Ceramic membranes were later employed in pilot-scale ultrafiltration of kraft black liquor, yielding SKL fractions of low molecular weight, free of sugars, and high sulfur content. No significant differences in carboxylic acid content were noted.[65] A correlation was observed between molecular weight and hydroxyl type: high molecular weight fractions had more aliphatic hydroxyls, while low molecular weight ones had more phenolic groups.[66] A three-stage ultrafiltration of Eucalyptus kraft liquor confirmed that progressively smaller cut-offs yielded purer fractions with dispersions as low as 1.1 and reduced hydroxyl content.[67] To mitigate membrane fouling, one of the great limitations of the present technology, microfiltration pre-treatment has proven effective, particularly with steam-exploded green wood lignin.[68] Recently, graphene oxide membranes have shown promise for selective retention of phenolic compounds, enabling tunable separation *via* steric effects.[69]

More recently, the segmented continuous flow fractionation technique (SCFF) was introduced by Majdar *et al.* focusing on SKL and wheat straw organosolv lignins.[70] SCFF is based on the fractional dissolution under dynamic conditions – varying solvent polarity, temperature, pressure, and flow rate – combined with real-time in-line monitoring *via* photodiode array and refractive index detectors. A standard HPLC setup was used, allowing for straightforward laboratory implementation and scalability (Fig. 8).

The method was initially applied to SKL using acetone, successfully separating acetone-soluble and acetone-insoluble fractions. Comparable or better results were achieved while comparing the SCFF method to traditional Soxhlet and precipitation-based methods, with ASKL rich in phenolic hydroxyl groups and AIKL representing a higher molecular weight, less soluble, fraction. Similar approaches using methanol showed broader but chemically distinct fractions, highlighting the potential to separate SKL based on interactions based on hydrogen bonding and polarity rather than just molecular weight. Solvent gradients (mixtures of variable composition in hexane/acetone) and temperature control (heating to 70 °C with back-pressure regulation) were used to improve

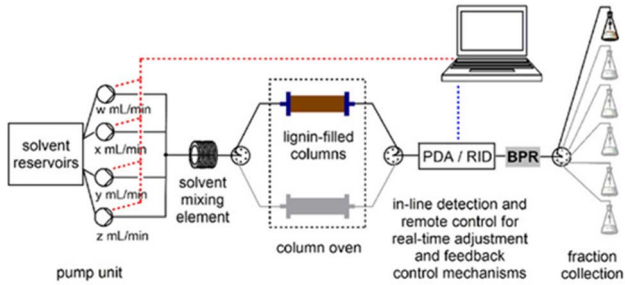

Fig. 8 Schematic flow scheme of the segmented continuous flow fractionation technique (SCFF) for lignins, with facultative, eventually PC-controlled, column exchange mechanism for scale-up. Reproduced from ref. 70 with permission from Wiley, copyright 2020.

separation resolution. Elevated temperatures significantly enhanced fraction differentiation and process efficiency without compromising results.

When SCFF was applied to wheat straw organosolv lignin, which is more complex due to its hydroxyphenyl/guaiacyl/sinapyl structure and higher impurity content, successful results were obtained. In the present case, methanol and ethanol–water systems were used to fractionate the substrate, with temperature and flow rate variations ensuring fractionation performance. Notably, ethanol gradients yielded distinct fractions, and a purification protocol using sequential organic solvents helped to isolate impurity-enriched and lignin-rich fractions. GPC and ^{31}P NMR confirmed the success of SCFF in separating fractions with varied molecular weights and functional group compositions. The approach was further patented by the same authors, describing also its applicability to a wide range of technical lignins.[71]

4. From lignin self assembly to nanoparticle nucleation & growth[72,73]

The drive to valorise lignin has emerged as a central objective in the pursuit of a sustainable, circular economy.[74] However, realizing the full potential of lignin remains a considerable challenge, largely due to its intrinsic chemical complexity and the wide array of extraction and fractionation methodologies employed to isolate this biopolymer.

Historically, the conversion of lignin into value-added products has proven difficult, primarily due to two fundamental issues: its extensive heterogeneity and structural diversity.[39,75] This variability stems from the absence of a well-defined primary structure, the presence of numerous inter-unit linkages distributed in a random fashion, and inherent botanical differences.[1,76,77] Further variability arises from the type of biomass (*e.g.*, wood or herbaceous plants), as well as the specific processing methods and severity used during isolation.[78–81]

The three-dimensional nature of lignin contributes to its polydisperse character, generating complex mixtures of oligomeric and polymeric constituents. These components occur in different proportions, which are highly dependent on the degree of degradation undergone during processing (H-factors).[82–85] A substantial body of literature has explored the behaviour of lignin in solution,

though interpretations remain varied due to its unpredictable and intricate interactions in both aqueous and organic solvents. A single lignin sample may contain a multitude of functional groups – such as phenolic, carboxylic acid, and aliphatic moieties[86–88] – each present in varying concentrations and exhibiting distinct acid dissociation constants.[89] Moreover, the presence of carbonyl functionalities and aromatic systems,[77] introduces further complexity, creating multiple sites for inter- and intramolecular interactions of differing thermodynamic stability, depending on the surrounding environment.[90] This complexity means that parameters such as pH,[91] ionic strength,[92] and dielectric constant,[93] can significantly influence lignin's behaviour in solution. Under specific conditions, lignin molecules adapt their conformation to achieve thermodynamic stability, leading to shape alterations and interaction patterns that may result in the formation of colloidal suspensions or larger aggregates, depending on whether the interactions are associative or repulsive.

Recent advancements in our understanding of lignin structure, combined with insights into the physical and chemical principles governing oligomeric and polymeric species, have paved the way for innovative strategies to manipulate lignin on the nanoscale. One such approach is to harness lignin's natural propensity to self-associate and aggregate.[94] By leveraging this behavior, researchers have begun to produce lignin nanoparticles, which enable enhanced compatibility with other matrices and promote the spatial arrangement of functional groups – achieved without resorting to chemical modification.[95]

The emergence of lignin nanoparticles with unique properties was initially unexpected, but it has since spurred considerable interest due to their potential in a wide range of applications. These include stimuli-responsive drug delivery systems,[96] food packaging,[97] antioxidants,[98] UV-vis shielding barriers,[99] *etc.* The functional properties of these nanoparticles are closely tied to their size, morphology, and hydrophobicity. Ongoing research is focused on optimizing these parameters to develop advanced, stimuli-responsive materials with superior performance characteristics.

4.1 Lignin inter and intramolecular interaction sites

The tendency of lignin to aggregate arises from a complex interplay of both intra- and intermolecular forces. The methods employed to extract lignin exert a profound influence on its structural characteristics, most notably on the distribution of molecular weights and the abundance of hydroxyl functionalities (see Table 2 for representative values). These structural differences, in turn, significantly affect the solubility of lignin and its aggregation profile, particularly *via* mechanisms such as hydrogen bonding and π–π stacking interactions (as illustrated in Fig. 9).

The interunit bonding patterns of native lignins are: aryl-glycerol-β-aryl ether (β-O-4′),[100–102] phenyl-cumarane (β,5′),[103] pinoresinol (β,β′),[104] dibenzodioxocyn (DBDO),[105,106] diphenyl (5–5′)[107,108] and diaryl ether (4-O-5′).[107] Aliphatic hydroxyl groups represent the most prevalent functional moiety (see Table 2), while the concentration of phenolic hydroxyl groups typically ranges from 0.9 to 2.0 mmol g^{-1}. In contrast, the content of carboxylic acid groups is relatively low, ranging between 0.01 and 0.05 mmol g^{-1}. The molecular weight of these species spans a broad range, approximately from 100 to 50 000 Da.

Table 2 Comparison of the average functional groups content, molecular weights & distribution for three technical lignins and milled wood lignin (MWL)

	Aliphatic OH (mmol g^{-1})	Phenolic OH (mmol g^{-1})	Carboxylic OH (mmol g^{-1})	Sulfonic groups (mmol g^{-1})	M_n (Da)
Kraft[75,83,116,117]	1.2–2.6	2.8–3.8	0.1–0.3	—	600–7000
Organosolv[118,119]	1.3–2.8	0.8–2.8	0–0.05	—	1200–2000
Lignosulfonate[115,120]	1.8–4.4	0.6–2.8	0.1–0.4	1.1–2.0	500–15000
MWL[77,85]	3.4–4.9	0.9–2.4	0.01–0.05	—	300–3000

Kraft-process-derived technical lignins undergo extensive structural alterations compared to the native lignin in wood. During this treatment, a number of original structural elements are significantly diminished, while new functional groups are introduced. These include aryl enol ethers, stilbenes, carboxylic acids, 1,4′-condensation sites, as well as ethoxy and thio-functionalities.[83] In contrast, the arylglycerol-β-aryl ether (β-O-4′) linkages (the most abundant interunit bonds in native lignin) are found to be significantly diminished in kraft lignin.[83] More

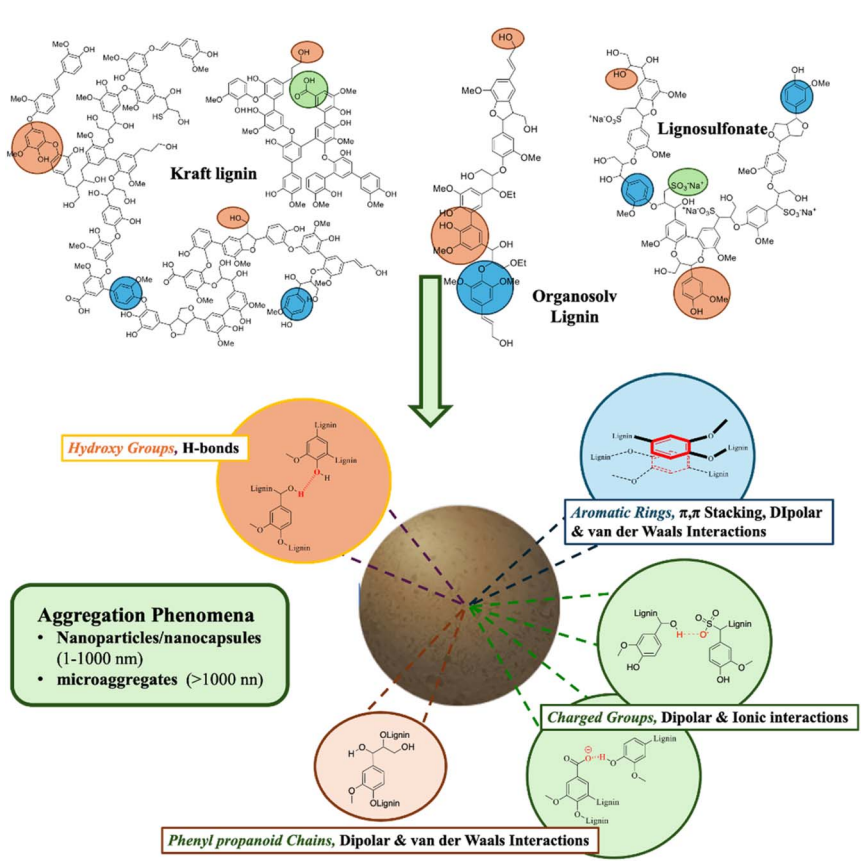

Fig. 9 Sites for inter/intramolecular association highlighted in technical lignins. Reproduced from ref. 72 with permission from Nature, copyright 2024.

broadly, kraft lignin is marked by a notable rise in free phenolic and carboxylic acid groups, coupled with a decline in aliphatic hydroxyl content when compared to its native wood-derived counterpart.[109–113] Organosolv lignin, by comparison, exhibits a narrower molecular weight distribution than kraft lignin, and retains a substantial proportion of the alkyl–aryl ether bonds – especially the β-O-4′ linkages – originally present in wood.[114] Consequently, organosolv lignin is generally considered less hydrophilic than its kraft counterpart.

Lignosulfonates, however, differ markedly from both kraft and organosolv lignins. Their structure is characterized by a high degree of hydrophilicity, due to the abundant presence of sulfonic acid groups attached to the aliphatic side chains.[115] Additionally, lignosulfonates possess a higher molecular weight compared to other technical lignins.

4.2 Self-assembly processes in lignin

Lignins can be broadly categorised into distinct domains based on their degree of polarizability (see Fig. 9). Polar regions typically consist of functional groups such as phenols, hydroxyls, carboxyls, and sulfonates, whereas the aromatic rings largely contribute to the polarisable character of the structure. In contrast, non-polarisable segments are primarily associated with the alkylated chains of the phenylpropanoid backbone.

This intricate network of bonding motifs and functional groups facilitates a wide spectrum of intermolecular interactions. These range from long-range forces – including van der Waals attractions, electrostatic effects, and hydrophobic interactions – to short-range contacts such as hydrogen bonding and π–π stacking. Collectively, these interactions govern the diverse aggregation behavior observed in lignin systems.[121]

Hydroxyl groups – whether aliphatic, phenolic, or part of carboxylic acids – are capable of forming hydrogen bonds and, in their deprotonated state, engaging in dipolar or electrostatic interactions. Meanwhile, sulfonate groups, owing to their polarity, tend to promote ionic and dipolar associations. Aromatic rings, due to their quadrupole moments, contribute to π–π stacking through quadrupolar interactions, further influencing lignin's aggregation characteristics.[92,121–124]

4.3 Lignin solubility

Lignin may be dissolved in either organic solvents or alkaline aqueous media, each exhibiting distinct solvation behaviours. Its solubility characteristics are effectively examined using the Hildebrand and Hansen solubility parameters. The Hildebrand parameter (δ_t) represents the energy necessary to disrupt the intermolecular forces within a substance to enable solvation, whereas Hansen's approach further refines this by partitioning the total solubility parameter into contributions from dispersive forces (δ_D), dipolar interactions (δ_P), and hydrogen bonding (δ_H).[125–127]

Solvents possessing a Hildebrand solubility parameter close to 22.5 $MPa^{1/2}$ have been identified as particularly suitable for dissolving lignin.[126] A notable example is dimethyl sulfoxide (DMSO), which has a Hildebrand value of 26.7 $MPa^{1/2}$. However, the Hildebrand parameter alone does not always provide a complete picture; for instance, DMSO proves to be a more effective solvent for lignin than 1-butanol, despite the latter having a Hildebrand parameter closer to

the ideal value of 22.5 $MPa^{1/2}$ (1-butanol $\delta_t = 23.2$ $MPa^{1/2}$). According to Hansen parameters, DMSO's superior solvency is primarily attributed to its stronger polar interactions (δ_P) rather than its hydrogen bonding capacity (δ_H).

Interestingly, a solvent's polarity does not directly equate to improved lignin solubility. It has been shown that DMSO's intermediate polarity, when compared with other solvents, induces the most significant expansion of lignin's polymeric chains.[88,121,128–130]

The solution behaviour of lignin may be partially interpreted through the Flory–Huggins theory.[93] More specifically, one can relate the radius of gyration (R_{gyr}), to the degree of polymer solvation and its molecular weight (M_W) through the following relation:

$$R_{gyr} \propto M_W^{a}$$

Here, the parameter a denotes the effectiveness of lignin solvation in the solvent under investigation. Under Θ conditions, a approaches the value of 0.5, indicating a balance between lignin's intermolecular forces and solvent–polymer interactions. In such a state, lignin and solvent are miscible without preferential interactions. When a falls below 0.5, dissolution occurs but remains limited. Conversely, when a exceeds 0.5, the solvent is highly effective, causing significant polymer expansion and greater surface exposure to the surrounding medium.

By employing molecular simulations, the Flory–Huggins model can be extended to lignin systems, allowing for the prediction of optimal solvents under defined conditions. DMSO has emerged as a particularly effective solvent, as it induces the most extensive conformational expansion in lignin chains, thereby exposing a larger surface area to solvation. This behavior has been modelled and validated across various lignin sources, including spruce, birch, and miscanthus, and shown to correlate with their inherent structural characteristics.[93] Among solvents examined, water exhibits the lowest a value, encouraging highly compact

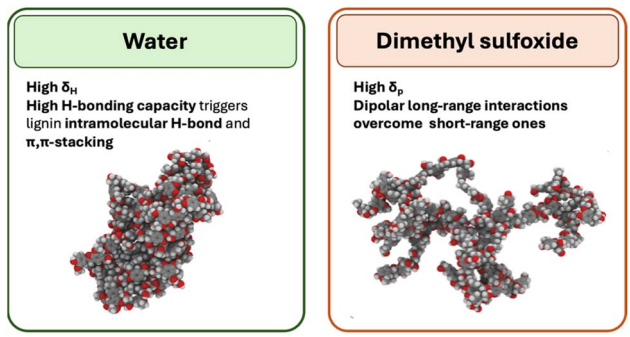

Fig. 10 A molecular simulation of lignin conformation in water and DMSO, respectively, has been reported.[93] The high hydrogen-bonding parameter (d_H) of water, indicative of strong short-range hydrogen bonding, enhances intramolecular π–π stacking and hydrogen bonds within lignin, thereby promoting a collapsed molecular configuration. In contrast, the high polarity parameter (d_P) of DMSO facilitates extended dipolar interactions between lignin and the solvent, favoring an elongated conformation. Reproduced from ref. 72 with permission from Nature, copyright 2024.

molecular conformations. A visual comparison of lignin aggregation behavior in DMSO *versus* water is illustrated in Fig. 10.

Radial distribution functions (RDFs) serve as a vital analytical tool for evaluating the extent and nature of interactions between solute and solvent molecules. Crucially, distinct functional groups within lignin contribute differently to these interactions. Hydroxyl groups, for instance, can form hydrogen bonds with solvent molecules, leading to the emergence of a hydration shell around specific chain segments in the lignin polymer. This phenomenon can reduce the likelihood of intramolecular contacts. Simultaneously, unbound hydroxyl groups may still participate in intramolecular hydrogen bonding. Hence, understanding the location and type of OH groups along the lignin backbone is essential for deciphering solvent–lignin interactions.[93]

Interestingly, the solubility of softwood kraft lignin has been shown to inversely correlate with the polarity of the solvent employed. The origin of lignin plays a critical role, as it dictates the composition and quantity of phenylpropanoid units, which in turn influence both intra- and intermolecular bonding behaviour.[77] For example, softwood lignin, which predominantly features guaiacyl (G-type) units, has only one methoxy group per aromatic ring.[131] This structural trait enhances the propensity for intramolecular hydrogen bonding and, as a result, improves the polymer's solvation capacity.[121,124] These structural insights lend support to the findings of Zwilling *et al.*,[132] who reported variations in lignin compactness depending on the solvent used. As solvent polarity decreases, lignin chains tend to adopt more extended conformations. Ultimately, lignin dissolution is governed not solely by the polymer's intrinsic properties but also by the solvent's characteristics – such as polarity, its nature as a protic or aprotic medium, and its capacity to interact with the polar functionalities within the lignin matrix.

4.4 Lignin aggregation

The self-assembly of lignin is primarily governed by subtle intermolecular and intramolecular interactions – particularly those involving hydroxyl functionalities and aromatic ring systems. A useful framework for understanding the interplay of these forces is the Derjaguin–Landau–Verwey–Overbeek (DLVO) theory, which connects the repulsive electrostatic potential between colloidal particles with parameters such as aggregate radius, surface charge potential, and interparticle distance, using the Debye length as a key descriptor.[132,133]

The size and colloidal stability of lignin nanoparticles are dictated by the delicate balance between long-range attractive van der Waals forces and short-range repulsive interactions stemming from the electrical double layer (EDL). Beyond these classical interactions, the molecular entanglement of lignin chains also significantly shapes their three-dimensional arrangement. Changes in the abundance and type of linkages – such as the aryl-glycerol-β-aryl ether units – have been directly associated with altered supramolecular behavior and aggregation tendencies.[121]

Lignin undergoes aggregation through a two-stage mechanism: an initial nucleation event followed by particle growth. Classical nucleation theory (CNT) describes this by positing that solute molecules in supersaturated solutions can reversibly form small, metastable clusters. Once these clusters exceed a critical

size, they become energetically favorable to grow and phase-separate from the medium as distinct entities.[134,135] In the case of lignin, primary nucleation arises from electrostatic interactions, leading to the formation of nanoscale aggregates. Subsequent particle enlargement occurs *via* a sequential, layer-by-layer accumulation of lignin macromolecules.[91,128,132,136,137]

Typically, the central core of such aggregates consists of higher molecular weight lignin fractions. Following initial sedimentation, lower molecular weight components deposit around the periphery of the aggregates.[132,136] While the nucleation stage is primarily dictated by lignin's inherent characteristics, the growth phase is modulated by the properties of the surrounding solvent.

Denser, more compact aggregate structures result from strong intramolecular forces, particularly π–π stacking between aromatic units. Guaiacyl (G-type) units exhibit stronger stacking capabilities than syringyl (S-type) units, leading softwood lignins – richer in G-units – to form tighter and smaller aggregates than their hardwood counterparts.[124,136,138,139]

Moreover, lignin's molecular architecture influences not only the particle size but also the morphology of resulting colloidal dispersions. For instance, hardwood-derived lignin tends to form elongated, densely packed rod-like aggregates, whereas softwood lignin generally forms cylindrical or shorter rod-shaped structures.[124]

Despite recent progress, our grasp of how lignin's structural nuances govern its interaction with various solvents remains incomplete and warrants further investigation. Emerging findings have shown that kraft lignin engages in hydrogen bonding when dissolved in ethylene glycol, whereas interactions with DMSO are dominated by dipole–dipole alignment and quadrupolar stacking.[91,136]

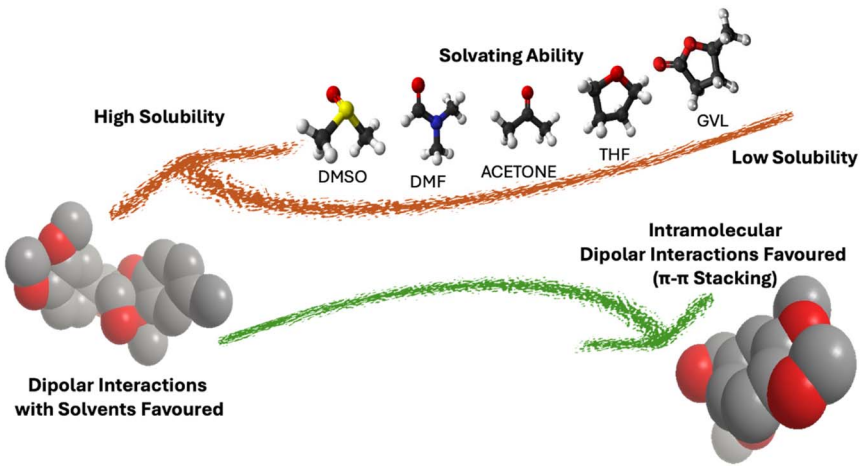

Fig. 11 As the solvating power of various solvents increases (left), dipolar interactions between lignin and the solvent are increasingly favored. Conversely, in solvents with lower solvating efficiency, intramolecular π–π stacking and hydrogen bonding within the lignin structure, dominate. Under such conditions, lignin adopts a more compact conformation in solution, and the subsequent introduction of water as an antisolvent promotes the formation of nanoparticles (right). Reproduced from ref. 72 with permission from Nature, copyright 2024.

The nature of the solvation medium significantly influences lignin–lignin association: in the case of alkali lignin, modifying the anti-solvent used can trigger aggregation through π–π stacking interactions. This phenomenon has been visually summarised in Fig. 11, which outlines a selection of solvents found to promote self-assembly *via* π–π interactions for arylglycerol-β-aryl ether dimers.[139]

Ultimately, the way lignin interacts with its surrounding solvent gives rise to diverse modes of aggregation, each yielding structurally distinct materials. The predominant technique for producing colloidal lignin involves solvent/antisolvent methodologies, whereby either an antisolvent is introduced into a lignin solution or the pH of an alkaline aqueous lignin mixture is reduced.[94,140,141]

Of particular note is the influence of the antisolvent's polarity, which enhances π–π stacking interactions.[121,136,139] Water, due to its poor capacity to solubilise lignin, has emerged as the most effective antisolvent. This aligns with earlier findings that associate water with the generation of compact, structurally defined aggregates. Consequently, employing water as an antisolvent proves to be a pragmatic strategy for synthesising lignin nanoparticles.[121,136,139] Salentinig and Schubert conducted a meticulous study into the role of water during aggregate formation in THF.[142] In pure THF, interactions are largely dictated by hydrogen bonding – especially among carboxylic and phenolic hydroxyl groups – as well as by quadrupolar π–π stacking. Small-angle X-ray scattering (SAXS) measurements revealed that aggregates formed under these conditions reached a minimum size of 6.4 nm. A sudden introduction of water, in a final 1 : 9 water-to-THF ratio, triggered the self-assembly of larger lignin aggregates than those observed in pure THF. This behaviour mirrors earlier reports attributing such aggregation to the sequential deposition of lignin layers, prompted by water's alteration of the π–π stacking interactions initially present in the solvent.[143] Comparable outcomes have been documented in the context of lignin nanoparticle formation *via* dialysis of lignin solutions in THF and ethylene glycol.[91] Notably, after thorough dialysis, the lignin aggregates stabilised in water, forming spherical nanoparticles of consistent morphology.

Lignin concentration plays a crucial role in modulating aggregation behaviour.[91,121,124,132,138] Elevated concentrations lead to increased molecular collisions and interactions, thereby promoting aggregate growth and initiating nucleation. This, in turn, produces a system with a broader size distribution.[91,138]

A threshold concentration – generally in the range of 1–3 g L^{-1} – is required to induce nucleation, though the exact value depends on the lignin's structural nature and rises with increased hydrophobicity.[132] Interestingly, at higher concentrations (5, 10, and 15 wt/vol%), aggregate sizes actually decrease, a trend attributed to the specific structural features of the lignin involved.[124]

Delving deeper, the stronger π–π interactions between guaiacyl (G) units – as opposed to syringyl (S) units – result in smaller aggregate formation from softwood lignin in comparison to that from hardwood sources. Furthermore, small-angle neutron scattering (SANS) analysis has shown that increased concentrations lead to the formation of fractal-like lignin nanostructures.[124]

The multifaceted dependence of nanoparticle dimensions on the diverse functional groups inherent in lignin is encapsulated in Fig. 12.[132,136,138,144]

The effect of pH on lignin aggregation has been comprehensively studied across numerous investigations.[121,128,133,142,145] At highly alkaline conditions,

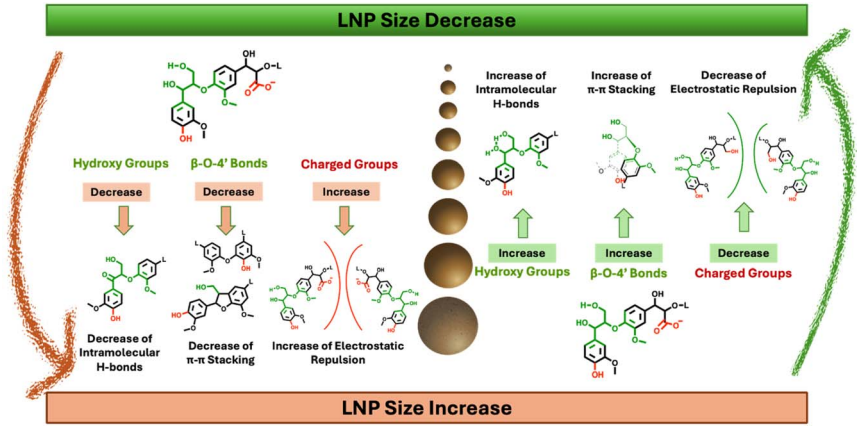

Fig. 12 The size of lignin nanoparticles (LNP) is influenced by several structural characteristics. A high concentration of hydroxyl groups promotes extensive intramolecular hydrogen bonding, which in turn leads to a more compact lignin conformation and the formation of smaller nanoparticles. Similarly, a greater abundance of β-O-4 linkages enhances π–π stacking interactions, also resulting in smaller particle sizes. The stronger π–π interactions associated with guaiacyl (G) units, as compared to syringyl (S) units, favour the production of smaller particles from softwood lignin. In contrast, the presence of charged groups – such as carboxylates – increases electrostatic repulsion between molecules, thereby encouraging the formation of larger particles. The dependence of lignin particle size on molecular weight is primarily attributed to variations in the distribution of aliphatic and phenolic hydroxyl groups across different lignins or lignin fractions.[132,136,138,144] Reproduced from ref. 72 with permission from Nature, copyright 2024.

particularly at pH values exceeding 13.8, lignin dissolves completely. Under such circumstances, interactions between solvent molecules and lignin, namely ionic-dipole forces and hydrogen bonding, supersede internal hydrogen bonding and π–π stacking between lignin chains.

A key factor in controlling lignin association and dissociation lies in the dissociation constants (pK_a) of its functional groups. For instance, carboxylic groups generally dissociate in the pH range 3–5, while phenolic hydroxyl groups dissociate between pH 8 and 11. Modulating the pH within these ranges enables precise control over the molecular interactions that underpin aggregation. This strategy has been employed in the design of 'smart' lignin-based materials for the targeted release of active substances.[128,145] The interplay between attractive forces (such as hydrogen bonds and π–π stacking) and repulsive electrostatic interactions – largely stemming from neighbouring anionic domains – ultimately governs both the size and stability of lignin aggregates. Notably, lignin nanostructures tend to form when the pH is adjusted downward from alkaline conditions (pH 8–11) to lower pH (5–8).[91,146,147]

The deprotonation of phenolic hydroxyl groups at alkaline pH imparts a negative charge to lignin, but upon acidification (pH 5–8), this charge is lost due to protonation, thereby triggering molecular rearrangement. At this pH range, protonated phenolic groups exhibit diminished hydrogen bonding, yet carboxylic groups remain largely deprotonated, retaining their anionic form. The resulting electrostatic repulsion – chiefly arising from adjacent carboxylate moieties – is believed to drive interparticle repulsion.[133]

Broadly speaking, lowering the pH of a lignin solution promotes aggregation, a consequence of changes in the electrical double layer due to altered ionisation states of lignin's functional groups. In much the same way, the ionic strength of the medium plays a critical role in directing aggregation.[91,146] As the ionic concentration increases, the thickness of the electrical double layer diminishes, thus facilitating aggregation.[146] The specific ions present can also profoundly influence colloidal lignin behaviour. According to the Hofmeister series, the following trend is observed for anions: $PO_4^{3-} < CO_3^{2-} < SO_4^{2-} < CH_3COO^- < HPO_4^{2-} < Cl^- < H_2PO_4^- < HCO_3^-$. Among cations, the hierarchy is: $Mg^{2+} < Ca^{2+} < H^+ < Na^+ < K^+$. Kosmotropic ions (those early in the series) tend to "salt out" nonpolar substances, reducing their solubility, whereas chaotropic ions (later in the sequence) enhance solubility. A predictive framework based on this series can assist in rationalizing and optimizing lignin colloidal stability across various environments.[92,148]

Temperature is another parameter that exerts a significant effect on lignin aggregation.[122,149,150] Elevating the temperature generally favors aggregation by increasing the rate of molecular collisions and reducing surface repulsive forces.[124,135,151]

4.5 Future outlook on lignin aggregation

Substantial progress has been achieved over the past decade in understanding lignin self-assembly.[90,121,152–154] What began as trial-and-error experimentation has evolved into research grounded in well-characterized molecular interactions between lignin chains and their solvent environment. When these insights are paired with the inherent chemical and polymeric properties of lignin, such as monomer composition, hydroxyl and methoxy substitution patterns, and molecular weight, they offer the potential to predict the characteristics of the resulting lignin-based nanomaterials.

Nevertheless, the inherently complex nature of lignin and its heterogeneous aggregation behavior remain significant obstacles, exacerbated by a lack of standardisation across experimental methodologies. Discrepancies in techniques for determining lignin structure, molecular weight distribution, and particle sizing make it difficult to compare data across studies. To address these issues, standardized approaches and robust fractionation protocols are essential. Uniform lignin fractions could help to reduce the inconsistencies frequently observed in aggregation studies.

This work has sought to delineate the key parameters influencing lignin self-assembly. Classical DLVO (Derjaguin–Landau–Verwey–Overbeek) theory has been employed to interpret the balance of long-range attractive van der Waals forces and electrostatic repulsion.[90,133] However, a comprehensive quantitative understanding of the contribution of short-range attractive forces – particularly hydrogen bonding – is still lacking.

One illustrative example of this knowledge gap is the absence of quantitative models describing the role of hydrogen bonding among aliphatic, phenolic, and carboxylic hydroxyl groups in lignin. Some headway has been made through studies on acetylated lignin, which revealed that while aliphatic and phenolic groups played a minor role, non-acetylated carboxylic acids were central to aggregation *via* hydrogen bonding.[91] Future efforts should strive to quantify the

roles of not only hydroxyl groups, but also molecular weight, steric hindrance, and π–π interactions. A molecular-level understanding of these contributions could clarify the primary driving forces behind lignin aggregation – still a subject of debate.[90] Clarifying the balance of attractive and repulsive forces would significantly enhance our ability to design and control self-assembly strategies. Moreover, further investigation is warranted into the role of solvents and non-solvents in aggregation. Understanding lignin's solvation and desolvation behavior is key to elucidating how final aggregate structures are shaped. Solvent polarity, in conjunction with the origin and processing history of the lignin (technical *versus* native), should be systematically explored to develop robust structure–property relationships. Similarly, the sequence and rate of component addition in nanoparticle preparation may critically influence assembly outcomes.

Finally, the fabrication of lignin nanoparticles offers a route to overcome many limitations of raw lignin, often without the need for environmentally harmful chemical modification. However, the environmental implications of lignin nanoparticle production remain underexplored. Many studies promoting the use of lignin nanomaterials fail to consider the full sustainability profile of the processes involved. Rigorous life-cycle assessments, accounting for yields, solvent usage, and other ecological metrics, would provide essential validation for the green credentials of lignin-based nanotechnologies.

5. Applications of lignin based micro- & nanomaterials

Lignin-based nanomaterials have emerged as a sustainable and cost-effective alternative to petroleum-derived products, showing great promise in agriculture, cosmetics, food packaging, and biomedicine, where stringent quality standards apply.[73] In agriculture, lignin nano-carriers offer an eco-friendly option for the controlled release of nutrients and agrochemicals. In fact, traditional polymeric capsules raise environmental concerns due to microplastic pollution. Alternatives include lignosulfonate-based hollow nano-capsules for hydrophilic compounds,[155] and acetylated alkali lignin colloidal spheres for pesticide delivery.[156] Hybrid systems enhance performance, such as aminated kraft lignin on magnetite nanoparticles enabling recyclable phosphorus and iron fertilizers.[157] Cosmetic applications benefit from the UV-absorbing properties of lignin, owing to its conjugated aromatic structure with absorption peaks around 280 and 300 nm. Lignin nanoparticles dispersed in oil-emulsions have proven effective UV screens.[99,158] Enhancements of the light-absorption were achieved by combining lignin with UV-active materials, such as in the case reporting the use of lignosulfonate-modified titania nanoparticles.[159] In food packaging, lignin nanoparticles enhance polymer matrices by improving mechanical strength, gas barrier properties, and UV protection.[97] Specifically, their integration into materials like poly-vinyl alcohol and polylactic acid has shown significant improvements up to 35% in tensile strength and 400% in elongation at break.[160] To address compatibility issues, chemical modification of lignin, such as citric acid esterification, were used to increase nanoparticle hydrophobicity, enabling higher loadings in polymeric matrixes and enhanced antioxidant activity.[161,162] In the field of biomedical applications, pH-responsiveness and biocompatibility of

lignin make it ideal for drug delivery systems. Studies have demonstrated the controlled release of hydrophilic drugs using lignosulfonate microcapsules,[163] alkali lignin nanoparticles,[164] and precipitation techniques.[165] Notably, lignin micelles have been developed for pH-dependent ibuprofen release, showing minimal release in gastric fluid and full release under intestinal conditions.[166] Hybrid lignin–magnetite nanoparticles have also been reported owing to their promising behavior for cancer diagnostics and therapy through magnetic targeting.[167]

In conclusion, lignin-based micro- and nano-materials offer multifunctional capabilities, positioning them as sustainable and adaptable platforms across various high-value sectors.

6. Rheological, anti-oxidant & mechanical behaviour of lignin & its fractions in polymer blends

Questions remain regarding the behaviour of SKL fractions compared to the unfractionated material. To explore this at a macroscopic level, the antioxidant properties and melt stability of polyethylene (PE) blended with both fractionated and unfractionated SKL were investigated. Notably, methylation of phenolic hydroxyl groups was found to significantly enhance the thermal stability of lignin/PE melts. However, more detailed analyses revealed that the individual ASKL and AIKL fractions exhibit markedly different behaviours from the original, unfractionated lignin.

The methylated ASKL, characterized by its low molecular weight and likely spherical morphology, unexpectedly acted as a plasticizer in PE melts. In contrast, the higher molecular weight AIKL contributed to greater melt stability, likely due to its rigid structure and higher glass transition temperature, potentially resulting from π–π interactions among its aromatic units. When ASKL and AIKL were combined, the resulting PE blends showed poor thermal stability and a strong tendency to undergo cross-linking in the absence of methylation.

These findings reveal, for the first time, a non-productive cooperative interaction between distinct SKL fractions, with significant implications for material performance and process design. This phenomenon was thoroughly examined by Sadaghifar,[168] who isolated the acetone fractions of SKL and evaluated their antioxidant capacity using the DPPH (2,2-diphenyl-1-picrylhydrazyl) radical scavenging assay. Among the samples, ASKL displayed the highest antioxidant activity, outperforming both unfractionated SKL and AIKL. This was reflected in the IC_{50} values – the concentration needed to inhibit 50% of DPPH radicals – which were lowest for ASKL (145.7 mg L^{-1}), followed by unfractionated lignin (166.1 mg L^{-1}), and highest for AIKL (223.2 mg L^{-1}). Similarly, the antioxidant activity index (AAI) ranked highest for ASKL (0.68), then SKL (0.6), and lowest for AIKL (Fig. 13).

Further confirmation came from ^{31}P NMR spectroscopy, which showed a strong correlation ($R^2 = 0.9721$) between phenolic hydroxyl content and antioxidant activity, with ASKL exhibiting the highest concentration of phenolic OH groups (5.76 mmol g^{-1}).

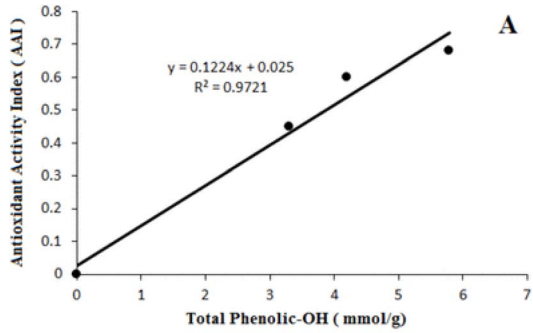

Fig. 13 Correlation of phenolic hydroxyl group content with the antioxidant activity index of SKL and its fractions. Reproduced from ref. 168 with permission from the American Chemical Society, copyright 2015.

The selective methylation of the phenolic hydroxyl groups with dimethyl sulfate of SKL, ASKL, and AIKL and the resulting methylated lignin were analysed *via* DPPH test, revealing that the antioxidant activity was abolished in all cases, unequivocally demonstrating the critical role of these functional groups.

The antioxidant performance of lignin–polyethylene (PE) blends was assessed by measuring the oxidation induction temperature (OI_{temp}), which reflects the material's resistance to thermal oxidation. Incorporation of SKL and ASKL led to a marked increase in the OI_{temp} of PE blends (Fig. 14).

Mechanistically, the stabilizing effect depended significantly on the lignin loading level. At concentrations below 5 wt%, the enhancement in OI_{temp} was attributed to the antioxidant activity of phenolic hydroxyl groups. At higher loadings (up to 25 wt%), thermal stabilization was instead linked to the formation of lignin-derived char, indicating a shift in the dominant mechanism.

AIKL demonstrated a comparatively weaker stabilizing influence. The differences in OI_{temp} across the various lignin fractions were strongly correlated with their phenolic hydroxyl group content, which underpins their antioxidant

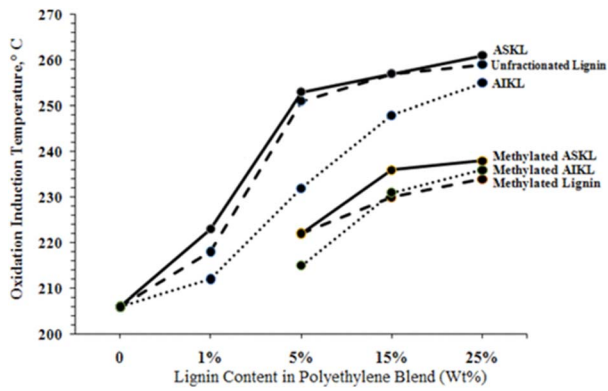

Fig. 14 Correlation of lignin content (unfractionated SKL and its fractions) in PE-blends with OI_{temp}. Reproduced from ref. 168 with permission from the American Chemical Society, copyright 2015.

properties. ASKL, possessing the highest concentration of phenolic hydroxyl groups, delivered the most significant improvement in OI_{temp}.

Not only the thermal behaviour of synthetic polymers is affected when blended with lignin and its fractions, but also their rheological properties. In fact, in another recent study,[169] the melt stability of PE blends with SKL and its acetone fractions was assessed *via* extruder torque tests (Fig. 15). PE blended with SKL resulted in a significantly increased initial and processing torque, testifying to thermal polymerisation coupled with cross-linking processes. The latter align with previous findings demonstrating an increase in the melt flow index of polyolefin–lignin blends depending on lignin content.[170]

In the case of ASKL, both methylated and unmethylated, extruder torque tests revealed significant differences in melt stability compared to pristine SKL (Fig. 15). Specifically, when incorporated into PE in a range comprised between 1 to 25 wt%, ASKL caused only minor increases in torque, suggesting an enhancement of the melt stability. Despite the higher phenolic OH content of ASKL than SKL, it was less prone to undergo cross-linking processes. This fact derives from both its lower molecular weight ($M_w = 3500$ g mol^{-1}) and narrower dispersion, limiting the likelihood of network formation during melt processing, according to the Flory–Stockmayer view that larger polymer chains require fewer cross-linking events to form a network structure.[171–173] The selective phenolic hydroxyl group methylation of ASKL resulted in an enhanced stabilization of the melt and introduced a distinct plasticizing effect. Specifically, the initial extrusion torque values were reduced by 8%, 18%, and 26% at 5%, 15%, and 25% loadings, respectively. This plasticizing effect was attributed to the low molecular weight and potentially spherical configuration of ASKL in solution, as suggested by considering the application of Kuhn–Mark–Houwink–Sakurada equations to kraft lignin.[174]

AIKL displayed a markedly different profile. In fact, blending 25 wt% AIKL with PE resulted in a 13% increase in initial torque – much higher than that seen with ASKL – yet melt viscosity remained relatively stable over time, contrasting with the instability observed for SKL (Fig. 14). This derives from the higher rigidity and the

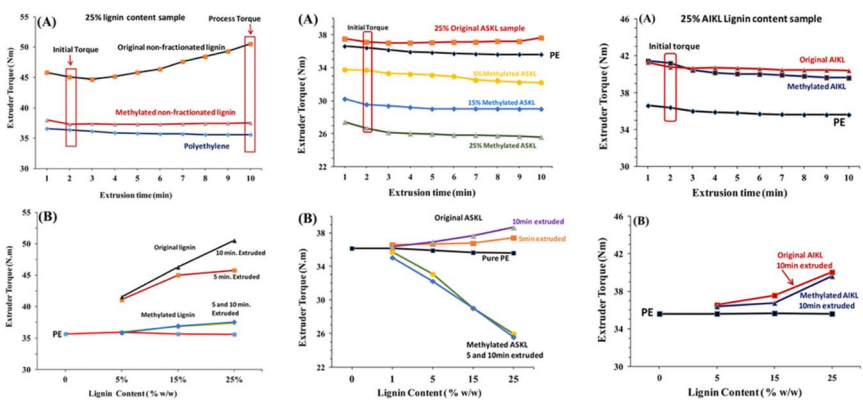

Fig. 15 Comparison of the extruder torque for SKL – polyethylene blends at different lignin loadings with SKL (left), ASKL (centre), and AIKL (right). Reproduced from ref. 169 with permission from the American Chemical Society, copyright 2016.

presence of π–π stacking interactions of AIKL,[175,176] imparting structural resistance against thermal cross-linking during processing. When the processing torque is compared for SKL and its fractions, relevant differences were evident, with SKL exhibiting a significant variability, while fractions offered more controlled behaviors. Consequently, the blend of the two fractions existing in SKL likely disfavors the π-stacking generated by AIKL due to the interference of spherical ASKL molecules, resulting in a random gelation and a greater melt torque fluctuations. Methylation of the fractions revealed an enhanced melt stability and plasticization, especially in the case of ASKL. In view of these results, the plasticizing effects were unequivocally attributed to its low molecular weight and spherical morphology which, despite the high phenolic content, reduced the chances of cross-linking. In fact, the gelation threshold in polymer melts is more sensitive to the molecular size of preformed chains than to functional group density alone.[171–173] Dimethyl sulfate methylation effectively blocks cross-linking and enhancing the ASKL compatibility with PE, improving processability. On the opposite side, the higher molecular weight of AIKL and its higher tendency to generate π,π-stacking interactions yields a more rigid structure, slightly raising initial torque but offering a more stable processing operation. Minor torque increases at higher loadings suggest that small-scale cross-linking can still occur.

An additional evaluation of the impact of blending 25 wt% SKL and its fractions on the mechanical properties of PE was performed *via* tensile tests (Fig. 16). In general, samples exhibited a reduced elongation at break compared to pristine PE, irrespective of methylation. However, methylated samples – particularly methylated ASKL – offered modest improvements in ductility, likely due to an improved phase compatibility between PE and ASKL upon methylation.[177,178]

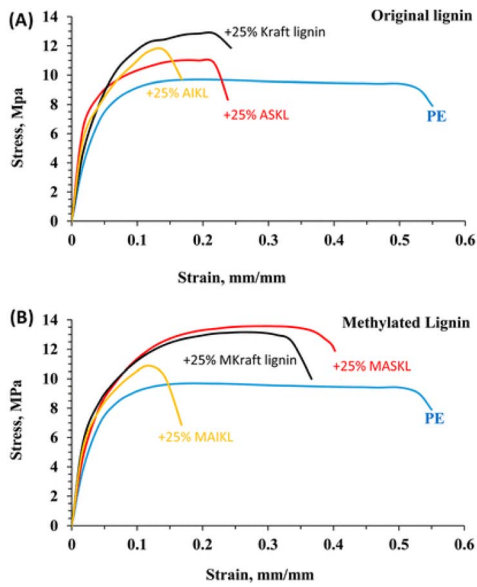

Fig. 16 Comparison of the stress *vs.* strain curves for SKL–polyethylene blends. Polyethylene blends were obtained for both unmodified (upper) and methylated (lower) lignin/fractions. Reproduced from ref. 169 with permission from the American Chemical Society, copyright 2016.

7. Lignin based carbon fibers

A very significant amount of research has been devoted to efforts producing carbon fibers from lignin, aiming at replacing traditional fossil-based raw materials. Despite its aromatic and polymeric nature, the heterogeneous, stochastic, and reactive characteristics of SKL seriously limit its potential for thermoplastic and carbon fiber applications. This is due to its low molecular weight and glass transition temperature causing it to soften during fiber formation and stabilization efforts. In addition, the lack of ordered structure within lignin hinders its graphitization that limits the attainment of the required moduli for carbon fibre materials.

In an effort to address the issue of low molecular weight and glass transition temperature of kraft lignin, Sen *et al.*[179] offered a novel route toward creating thermoplastic lignin polymers by exploring propargylation derivatization chemistry and its potential as a versatile novel route for the eventual utilization of technical lignins with a significant amount of molecular control. To do this, the systematic propargylation of SKL was explored and the versatile nature of the pendant propargyl groups on lignin was demonstrated *via* two distinct chain extension chemistries. Amongst them the most interesting was the solid-state, thermally induced, Claisen rearrangement polymerization chemistry displayed in Fig. 17.

Overall, it was shown that it is possible to modulate the reactivity of SKL *via* a combination of methylation and chain extension providing a rational means for the creation of higher molecular weight polymers with the potential for thermoplastic materials and carbon fibers with the desired control of structure–property relations.

Specifically, lignin was chemically modified by introducing reactive pendants on lignin moieties; subsequently, the latter are polymerised increasing the overall molecular weight of the starting lignin. The modification strategy involved both a fractionation operation and chemical modification.[179] Fractionation, as previously described, represents a core aspect, allowing for the isolation ASKL; the latter was chosen for its lower molecular weight and its higher content of phenolic

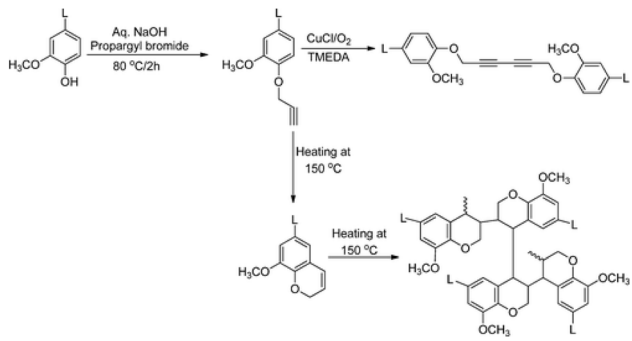

Fig. 17 Lignin chain elongation strategies. The lower part of this schematic displays the Claisen rearrangement and the ensuing thermal polymerization referred to in the text. Reproduced from ref. 179 with permission from the American Chemical Society, copyright 2013.

hydroxyl groups, making its functionalisation more selective and easier than the whole SKL. The selective propargylation of phenolic hydroxyl groups was then applied at different ratios of propargyl bromide/phenolic hydroxyl groups. Despite the heterogeneous reaction environment utilised, the quantitative functionalisation of phenolic hydroxyl groups was achieved without the need for an organic co-solvent. ^{31}P NMR spectra permitted the elucidation of the reactivity differences among the various types of phenolic hydroxyl groups present in ASKL towards propargylation. While non-condensed phenolic hydroxyl groups showed rapid substitution, condensed phenolic hydroxyl groups, such as diaryl ethers and biphenyls exhibited a more intricate reactivity pattern, likely affected by their higher steric hindrance than non-condensed ones. The thermal stability of the propargylated ASKL samples was evaluated *via* thermogravimetric analyses, demonstrating a significant improvement of the thermal stability even after 25% propargylation. Thermograms revealed broad exotherms between 150 and 215 °C, absent in pristine ASKL, which were attributed to the Claisen rearrangement and subsequent polymerisation of the aryl propargyl ether moieties.

In view of preparing precursors suitable for thermal operations, two distinct chain extension chemistries were explored by profiting from the presence of the propargyl groups on lignin. Namely, the copper-mediated oxidative coupling and the thermally induced polymerisation *via* Claisen rearrangement (Fig. 17). The solid state thermal polymerization of propargylated SKL offered tremendous possibilities for carbon fiber formation since the reaction requires no solvents and no volatile by-products are produced, that may eventually induce weak void points within the fibres.

One significant aspect of the proposed chemistry is that by initially methylating a fraction of the phenolic hydroxyl groups and then propagating the rest, one may modulate the degree of polymerization and thus avoid gelation (Fig. 18). Thermally induced polymerisation was directly conducted on 75% propargylated ASKL samples with 25% methylated residual phenolic hydroxyl groups. It was demonstrated that by heating the modified ASKL it was possible to induce a Claisen rearrangement, forming chromene structures. The latter subsequently polymerised *via* ene–ene homo-polymerisation yielding the effective chain

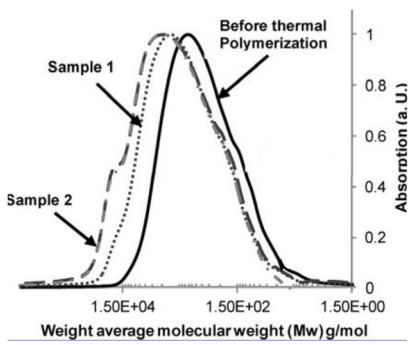

Fig. 18 Weight average molecular weight distributions of the methylated/propargylated SKL before and after the thermally-induced polymerization. Samples 1 and 2 were polymerized at 150 °C, for 10 and 60 minutes respectively. Reproduced from ref. 179 with permission from the American Chemical Society, copyright 2013.

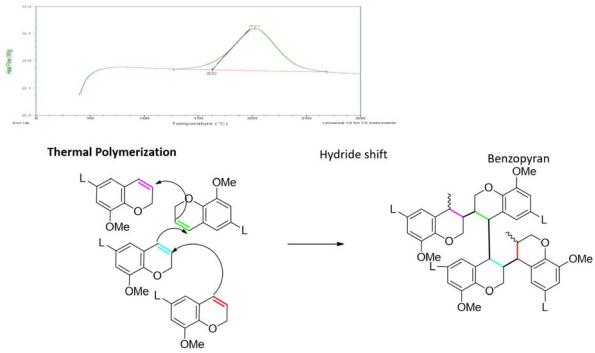

Fig. 19 Differential scanning calorimetry offers a convenient means to monitor the degree of thermal polymerization of the propargylated SKL by evaluating the developed exotherm depicted.

extension generating benzopyran domains. ^{13}C NMR analyses of the polymers showed new signals indicative of chromene formation as well as signals pertaining to the opening of double bonds during polymerisation.

One important aspect of this chemistry is that the polymerization of the pendant groups on the lignin can be monitored using differential scanning calorimetry (DSC). This is because the polymerisation events of the double bond present in the benzopyrane structures are exothermic reactions exhibiting broad DSC peaks in a temperatures range between 150 and 215 °C (Fig. 19).

The modulation of gelation *via* a controlled methylation followed by propargylation and thermal polymerization has resulted in the creation of single component carbon fibers made solely of SKL. Fig. 20A displays the fibers than can be pulled out of a melt of such lignins and prior to stabilization. Eventually,

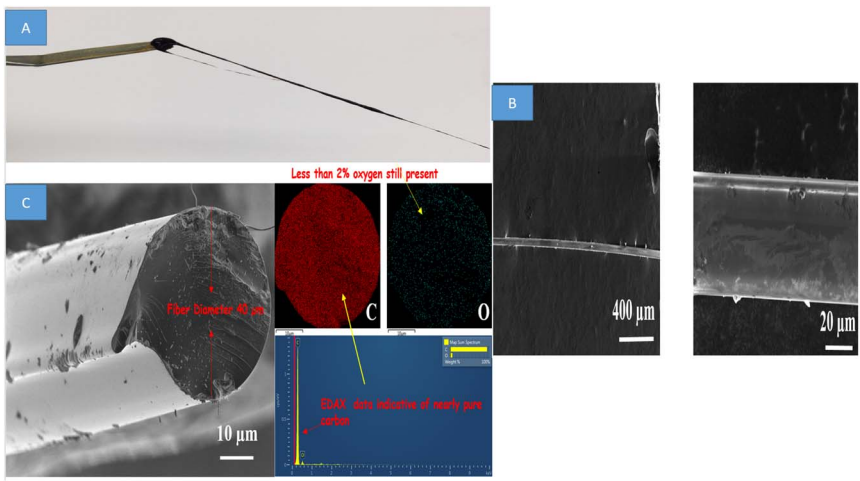

Fig. 20 (A) Showing fibers being pulled out of the melt from methylated/propargylated softwood kraft lignin; (B) photo-micrographs of fibers after carbonization; (C) cross-section & EDAX analyses of carbon fibers produced from methylated/propargylated SKL.

carbonization efforts produced fibers of various dimensions (Fig. 20B). It is to be noted that the thermal polymerization chemistry that produced no by-products offers fibers that are dense, free of voids of other defects, that may cause points of weakness within the fiber (see 40 micrometer fiber cross-section in Fig. 20C). Detailed EDAX analytical work shows that the carbonized fibers are composed mostly of carbon and less than 2% oxygen.

Besides the intrinsic limitations arising from the low molecular weight of lignin, the degree of graphitisation remains a major challenge in the production of lignin-based carbon fibres (CF). A critical survey of the topic was recently provided by Sagues *et al.*,[180] and asked the question: "Are lignin-derived carbon fibers graphitic enough?". Single component lignin-derived carbon fibers have been under development for many years, but strength properties are still inferior to those of commercial carbon fibers. The extent of graphitization is an overlooked limitation to lignin-derived carbon fiber development, particularly for high-modulus fibers treated at high temperatures.

The tensile moduli of commercial carbon fibers increase with temperature during graphitization, however, lignin-derived carbon fiber moduli stay the same or decrease (Fig. 21A).

In their review Sagues *et al.*[180] discuss the inability of lignin-derived carbon fibers to graphitize in a manner similar to commercial carbon fibers based on the irregular structure of lignin. In general, and as it becomes apparent from the above figure, single-component lignin CF perform significantly worse than

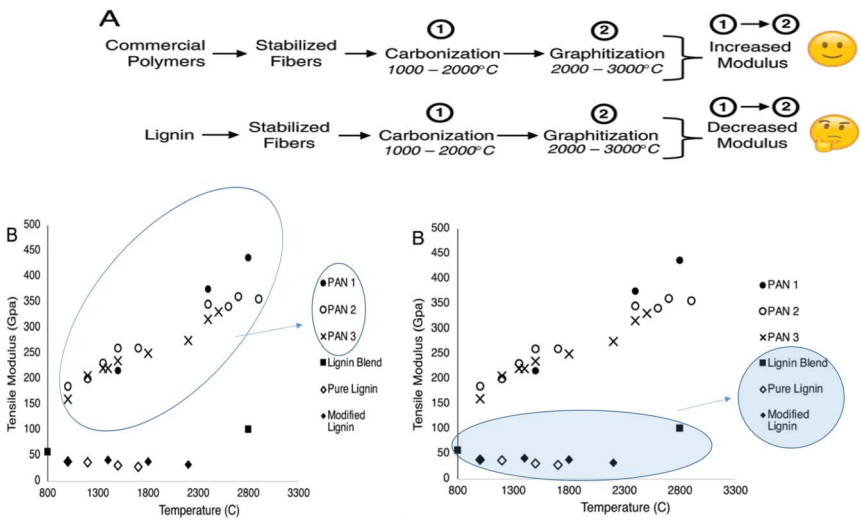

Fig. 21 (A) Schematic conveying an overlooked discrepancy in the temperature–modulus relationship among lignin-derived and commercial carbon fibers. (B) Plots showing the change in tensile modulus as a function of temperature for six carbon fibers (adapted from ref. 182–186): on the left, PAN 1, 2, & 3 refer to polyacrylonitrile carbon fibers treated at 1000–2900 °C;[182–186] on the right lignin blend data is shown – carbon fibers derived from pyrolysis fuel oil blended with hardwood kraft lignin treated at 800 and 2800 °C,[185] pure lignin: carbon fibers derived from SKL treated at 1000–1700 °C,[184] modified lignin: carbon fibers derived from acylated softwood lignin treated at 1000–2200 °C.[186] Reproduced from ref. 180 with permission from the Royal Society of Chemistry, copyright 2019.

polyacrylonitrile (PAN)-based fibres; however, lignin–PAN blends offer a viable route for the potential of lignin.[181]

In such blends, improvements in properties derive exclusively from the PAN component rather than lignin itself.[181,187,188] From a mechanistic perspective, it is a common but often unverified assumption, that lignin undergoes a structural transformation from disordered sp^3-hybridised to graphitic sp^2-hybridised carbon. Although X-ray diffraction and Raman spectroscopy analyses have been performed, there is insufficient evidence to support the present hypothesis. Impurities, fibre morphology, and defects are often cited as causes for the poor performance of lignin-derived CF,[181] while the critical issue of insufficient graphitic structure, particularly in high modulus carbon fibres (HMCFs), is frequently overlooked. This was recognised as early as 1951, when it was reported that highly cross-linked, three-dimensional polymers are poor precursors for graphitisation.[189] In this context, the thermal stabilisation stage plays a vital role in determining the achievable degree of graphitisation.[189] PAN serves as an excellent CF precursor due to its linear chains, which undergo cyclisation during thermal stabilisation.[190] The resulting cyclic structures facilitate graphitisation at elevated temperatures, producing HMCFs with ordered, ribbon-like graphitic domains interspersed with disordered regions.

Understanding the thermal behavior of lignin is complex. It is generally assumed that lignin undergoes condensation upon heating, with the nature of the linkages depending on lignin type.[191,192] Kraft lignin, the most studied lignin type, undergoes radical coupling reactions, creating carbon–carbon bonds restricting molecular rotation.[193] Upon heating to 500 °C, volatiles are released and oligomeric tars form, followed by side-chain decomposition and aromatic condensation at higher temperatures.[191,194] Above 800–1000 °C, aromatic ring opening can occur.[191,194] However, the irregular structure of lignin limits graphitisation compared to PAN, whose regular arrangement promotes the formation of sp^2 centres.[194,195] Consequently, lignin carbonisation remains poorly understood, complicating the production of highly graphitic CFs.

It is important to mention here that the graphitisation of lignin has been studied extensively. Highly graphitic structures have been reported for organosolv lignin-derived CF treated at temperatures up to 2700 °C, as derived from X-ray diffraction analyses, crystallite sizes, and reduced interlayer spacings.[196,197] Nonetheless, no corresponding increases in tensile modulus or strength were observed, suggesting lignin CF graphitise differently from PAN fibres. Whereas PAN fibres become graphitic around 1800 °C, lignin CFs remain disordered until much higher temperatures are reached. In fact, poor graphitisation of kraft lignin-derived CF has been observed at graphitisation temperatures up to 1700 °C.[198] Studies reported a limited increase in graphitic character for organosolv lignin-derived CF when treated at 2000 °C, as well.[199] In general, although Raman spectroscopy indicated some graphitic regions, these data may also misrepresent the bulk material. Recently, Köhnke demonstrated improved graphitisation when micro-size kraft lignin powders were treated at 2000 °C,[200] suggesting that particle size significantly influences graphitisation outcomes. A comprehensive mapping is still necessary to avoid misleading conclusions. Overall, the chemistry and thermal behaviour of lignin differ markedly from PAN, complicating efforts to produce highly graphitic, high-performance CFs.

Lignin fractionation seems promising in enhancing graphitisation. Jin *et al.* employed the ALPHA process to fractionate SKL by leveraging molecular weight *via* acetic acid–water liquid–liquid equilibrium.[201] CF produced from higher molecular weight fractions exhibited superior tensile strength and modulus, attributed to increased graphitic structure. Similarly, Liu used a pH-fractionation on corn stalk lignin; the resulting fractions were subsequently blended with PAN prior to the subsequent carbonization.[202] Fibres produced with higher molecular weight lignin – around 8200 g mol^{-1} – displayed a significantly enhanced elastic modulus (4.5 $\pm$ 0.1 GPa) compared to those from lower molecular weight lignin (2.6 $\pm$ 0.4 GPa). Although fractionation improves mechanical properties, lignin-derived CF still fall short of matching those of PAN-based CF. Nevertheless, further high-temperature treatment of fractionated lignins could foster even greater graphitisation and property enhancements, potentially enabling high-performance lignin-based CF at moderate carbonisation temperatures (<1500 °C).[201,203,204]

Most attempts to graphitise lignin have employed furnaces limited in temperature of approximately 1500 °C, suggesting the need for transition-metal catalysts to enhance graphitic structures at lower temperatures. In this regard, efficient graphitisation of hydrolysis lignin has been achieved using a nickel-based catalyst.[205] Two principal catalytic mechanisms have been proposed: carbon dissolution into nanosized particles followed by graphitic layering, and metal carbide formation followed by decomposition at high temperatures.[206] The use of methane and natural gas has also been shown to promote graphitisation during kraft lignin carbonisation, likely through vapour deposition on the catalyst surface.[194]

The surface decoration of CFs with carbon nanotubes *via* chemical vapour deposition has recently been reported to enhance thermal stability and conductivity, although this remains underexplored for lignin-derived CF.[207–210] Notably, the successful decoration of lignin–PAN CF with iron and palladium nanoparticles *via* chemical vapour deposition was recently demonstrated and verified by electron energy loss spectroscopy;[207] however, a systematic evaluation of the properties of the resulting materials is still needed.

8. Conclusions

Significant progress has been made in understanding the chemical mechanisms that govern lignin behaviour during pulping, shedding new light on the structural characteristics of kraft lignin. Combined with recent developments in lignin fractionation, these insights have paved the way for the formulation of a new structural model for SKL, which may support further research and industrial applications.

Despite these advances, technical lignin streams pose considerable challenges for replacing or supplementing petrochemical-based feedstocks. This difficulty stems from lignin's inherent variability, heterogeneity, coloration, and reactivity. Variations in feedstock due to seasonal changes, pulping conditions such as the H-factor, and related delignification processes, result in a complex and unpredictable mixture. Consequently, any lignin intended for downstream utilization must first be refined into products with consistent, well-defined specifications. This need parallels the treatment of crude oil, which, although initially suitable

only as a fuel, is refined into a wide array of chemicals that form the backbone of the petrochemical industry. Therefore, lignin refining or fractionation is essential and must be integrated into any industrial strategy for lignin utilization.

A deeper understanding of the roles played by solvents and non-solvents in lignin aggregation is also critical in lignin fractional precipitation. This includes studying the efficiency of solvation and desolvation processes and how they influence the shape and size of lignin particles. Important relationships between solvent polarity and different lignin types (*e.g.*, native *vs.* technical) may reveal valuable structural insights. Additionally, the rate and sequence in which components are added during aggregation should be carefully optimized, as these factors can significantly influence the assembly process.

Fundamental aspects of lignin self-assembly and the associated technological developments have attracted growing interest, especially in the context of producing high-value, sustainable nanomaterials for diverse applications. Considerable advancements have been made in identifying the key parameters that govern lignin self-assembly, particularly in terms of solvation behaviour in organic and aqueous systems. However, the lack of standardized methodologies for measuring lignin molecular weights, distributions, structural characteristics, and aggregate sizes, limits comparability across studies. Moreover, the specific contributions of hydrogen bonding – among aliphatic, phenolic, and carboxylic hydroxyl groups – remain poorly quantified. Future efforts should also take into account the roles of molecular weight, steric effects, and π–π interactions, in addition to hydroxyl group content. A comprehensive understanding of these factors could eventually clarify the main driving forces behind lignin self-assembly, where both attractive and repulsive interactions play a role. A clearer understanding of these interactions would significantly aid the optimization of aggregation strategies.

Another area of interest is the distinctive behaviour of lignin fractions when blended with polyolefins. It has recently been demonstrated that certain lignin fractions within SKL exhibit non-productive cooperative interactions, a phenomenon with important technological implications that deserves further exploration.

Significant strides have also been made in producing thermally stable lignin melts, with phenolic hydroxyl groups playing a key role in their stabilization. Nonetheless, a key question remains: can technical lignins, on their own, be effectively carbonized and graphitized to yield single-component, lignin-derived carbon fibers with mechanical properties that rival their fossil-derived counterparts?

Lastly, the broader environmental sustainability of lignin applications – including fractionation, nano-aggregation, and carbon fiber production – remains an open question. Many discussions on lignin utilization overlook key sustainability factors. Comprehensive life cycle assessments that account for product yields, solvent use, and other environmental parameters are crucial for lending credibility to lignin-based technologies and their claimed benefits.

Author contributions

N. P. and DSA contributed to the writing and the assembly of the various drafts of the text, C. C. and DSA conceptually and materially contributed to various

segments of the already published papers that the present review rests upon. All authors reviewed the manuscript.

Conflicts of interest

There are no conflicts to declare.

Data availability

The present review paper that pertains to the introductory lecture of the Frontiers in physical chemistry for lignin valorisation *Faraday Discussions*, contains data that has been previously published by the authors. No primary research results, software or code have been included and no new data were generated or analysed as part of this review.

Notes and references

1 K. V. Sarkanen, in *The Chemistry of Wood*, Interscience Publishers, New York, 1963, pp. 250–311.
2 W. Boerjan, J. Ralph and M. Baucher, *Annu. Rev. Plant Biol.*, 2003, **54**, 519–546.
3 *Lignin and Lignans*, ed. C. Heitner, D. Dimmel and J. Schmidt, CRC Press, 2010.
4 J. Ralph, C. Lapierre and W. Boerjan, *Curr. Opin. Biotechnol.*, 2019, **56**, 240–249.
5 D. D. S. Argyropoulos, C. Crestini, C. Dahlstrand, E. Furusjö, C. Gioia, K. Jedvert, G. Henriksson, C. Hulteberg, M. Lawoko, C. Pierrou, J. S. M. Samec, E. Subbotina, H. Wallmo and M. Wimby, *ChemSusChem*, 2023, **16**, e202300492.
6 O. Fearon, S. Kuitunen, K. Ruuttunen, V. Alopaeus and T. Vuorinen, *Ind. Eng. Chem. Res.*, 2020, **59**, 12977–12985.
7 J. Gierer, L.-Å. Smedman, G. Cederberg, R. B. Jensen, C. T. Pederson and E. Larsen, *Acta Chem. Scand.*, 1965, **19**, 1103–1112.
8 R. Kondo, Y. Tsutsumi and H. Imamura, *Holzforschung*, 1987, **41**, 83–88.
9 G. E. Miksche, A. Kjekshus, D. G. Mukherjee, A. T. Nicholson and J. T. Southern, *Acta Chem. Scand.*, 1972, **26**, 3275–3281.
10 S. Ljungagren, *Sven. Papperstidn.*, 1980, **83**, 31.
11 M. Ragnar, G. Henriksson, M. E. Lindström, M. Wimby, J. Blechschmidt and S. Heinemann, in *Ullmann's Encyclopedia of Industrial Chemistry*, John Wiley & Sons, Ltd, 2014, pp. 1–92.
12 J. Gierer, *Wood Sci. Technol.*, 1980, **14**, 241–266.
13 G. Gellerstedt and E.-L. Lindfors, *Nord. Pulp Pap. Res. J.*, 1987, **2**, 71–75.
14 M. Sette, R. Wechselberger and C. Crestini, *Chem.–Eur. J.*, 2011, **17**, 9529–9535.
15 D. Ibarra, M. I. Chávez, J. Rencoret, J. C. Del Río, A. Gutiérrez, J. Romero, S. Camarero, M. J. Martínez, J. Jiménez-Barbero and A. T. Martínez, *J. Agric. Food Chem.*, 2007, **55**, 3477–3490.
16 C. Crestini, H. Lange, M. Sette and D. S. Argyropoulos, *Green Chem.*, 2017, **19**, 4104–4121.

17 H. Sixta, H.-U. Süss, A. Potthast, M. Schwanninger and A. W. Krotscheck, in *Handbook of Pulp*, John Wiley & Sons, Ltd, 2006, pp. 609–708.
18 C. S. Lancefield, H. L. J. Wienk, R. Boelens, B. M. Weckhuysen and P. C. A. Bruijnincx, *Chem. Sci.*, 2018, **9**, 6348–6360.
19 A. Majtnerová and G. Gellerstedt, *Nord. Pulp Pap. Res. J.*, 2006, **21**, 129–134.
20 G. Gellerstedt, *Ind. Crops Prod.*, 2015, **77**, 845–854.
21 S. C. Fox and A. G. McDonald, *Bioresearch*, 2010, **5**, 990–1009.
22 A. Majtnerová and G. Gellerstedt, *Nord. Pulp Pap. Res. J.*, 2006, **21**, 129–134.
23 G. Gellerstedt, A. Majtnerova and L. Zhang, *C. R. Biol.*, 2004, **327**, 817–826.
24 N. Giummarella, P. A. Lindén, D. Areskogh and M. Lawoko, *ACS Sustainable Chem. Eng.*, 2020, **8**, 1112–1120.
25 N. Giummarella, I. V. Pylypchuk, O. Sevastyanova and M. Lawoko, *ACS Sustainable Chem. Eng.*, 2020, **8**, 10983–10994.
26 A. S. Hay and B. M. Boulette, *J. Org. Chem.*, 1976, **41**, 1710–1712.
27 M. Helander, H. Theliander, M. Lawoko, G. Henrikkson and L. Zhang, *BioResources*, 2013, **8**, 2270–2282.
28 J. Marton and T. Marton, *Tappi*, 1964, **47**, 471–476.
29 A. Jacobs and O. Dahlman, *Nord. Pulp Pap. Res. J.*, 2000, **15**, 120–127.
30 N. Pajer, M. Gigli and C. Crestini, *ChemSusChem*, 2024, **17**, e202301646.
31 A. Ház, M. Jablonský, I. Šurina, F. Kačík, T. Bubeníková and J. Ďurkovič, *Forests*, 2019, **10**, 483.
32 L. Dehne, C. Vila Babarro, B. Saake and K. U. Schwarz, *Ind. Crops Prod.*, 2016, **86**, 320–328.
33 Y. Zhao, A. Tagami, G. Dobele, M. E. Lindström and O. Sevastyanova, *Polymers*, 2019, **11**, 538.
34 J. Asikkala, T. Tamminen and D. S. Argyropoulos, *J. Agric. Food Chem.*, 2012, **60**, 8968–8973.
35 W. G. Glasser, V. Davé and C. E. Frazier, *J. Wood Chem. Technol.*, 1993, **13**, 545–559.
36 S. Kubo and J. F. Kadla, *J. Polym. Environ.*, 2005, **13**, 97–105.
37 O. Gordobil, E. Robles, I. Egüés and J. Labidi, *RSC Adv.*, 2016, **6**, 86909–86917.
38 C. Cui, R. Sun and D. Argyropoulos, *ACS Sustain. Chem. Eng.*, 2014, **2**, 959–968.
39 M. Gigli and C. Crestini, *Green Chem.*, 2020, **22**, 4722–4746.
40 C. Crestini, H. Lange, M. Sette and D. S. Argyropoulos, *Green Chem.*, 2017, **19**, 4104–4121.
41 X. Jiang, D. Savithri, X. Du, S. Pawar, H. Jameel, H. Chang and X. Zhou, *ACS Sustainable Chem. Eng.*, 2017, **5**, 835–842.
42 A.-S. Jääskeläinen, T. Liitiä, A. Mikkelson and T. Tamminen, *Ind. Crops Prod.*, 2017, **103**, 51–58.
43 X. Meng, A. Parikh, B. Seemala, R. Kumar, Y. Pu, C. E. Wyman, C. M. Cai and A. J. Ragauskas, *Bioresour. Technol.*, 2019, **272**, 202–208.
44 G. Wang, X. Liu, B. Yang, C. Si, A. M. Parvez, J. Jang and Y. Ni, *ACS Sustainable Chem. Eng.*, 2019, **7**, 10112–10120.
45 R. Sun, J. Tomkinson and J. Bolton, *Polym. Degrad. Stab.*, 1999, **63**, 195–200.
46 R. Sun, J. Tomkinson and S. Griffiths, *Int. J. Polym. Anal. Charact.*, 2000, **5**, 531–547.
47 S. I. Mussatto, M. Fernandes and I. C. Roberto, *Carbohydr. Polym.*, 2007, **70**, 218–223.
48 C. Schuerch, *J. Am. Chem. Soc.*, 1952, **74**, 5061–5067.

49 R. Ebrahimi Majdar, A. Ghasemian, H. Resalati, A. Saraeian, C. Crestini and H. Lange, *Polymers*, 2019, **11**, 225.
50 T.-Q. Yuan, J. He, F. Xu and R.-C. Sun, *Polym. Degrad. Stab.*, 2009, **94**, 1142–1150.
51 T. Saito, J. H. Perkins, F. Vautard, H. M. Meyer, J. M. Messman, B. Tolnai and A. K. Naskar, *ChemSusChem*, 2014, **7**, 221–228.
52 C. G. Boeriu, F. I. Fiţigău, R. J. A. Gosselink, A. E. Frissen, J. Stoutjesdijk and F. Peter, *Ind. Crops Prod.*, 2014, **62**, 481–490.
53 Z. Jia, M. Li, G. Wan, B. Luo, C. Guo, S. Wang and D. Min, *RSC Adv.*, 2018, **8**, 42269–42279.
54 K. Wang, F. Xu and R. Sun, *Int. J. Mol. Sci.*, 2010, **11**, 2988–3001.
55 R. W. Thring, E. Chornet, J. Bouchard, P. F. Vidal and R. P. Overend, *Ind. Eng. Chem. Res.*, 1991, **30**, 232–240.
56 R. W. Thring, E. Chornet and R. P. Overend, *Can. J. Chem. Eng.*, 1993, **71**, 116–123.
57 C. Liu, C. Si, G. Wang, H. Jia and L. Ma, *Ind. Crops Prod.*, 2018, **111**, 201–211.
58 M. Lawoko, G. Henriksson and G. Gellerstedt, *Biomacromolecules*, 2005, **6**, 3467–3473.
59 F. Zikeli, T. Ters, K. Fackler, E. Srebotnik and J. Li, *Ind. Crops Prod.*, 2016, **91**, 186–193.
60 X. Du, G. Gellerstedt and J. Li, *Plant J.*, 2013, **74**, 328–338.
61 G. Wang and H. Chen, *Sep. Purif. Technol.*, 2013, **120**, 402–409.
62 A. Toledano, L. Serrano, A. Garcia, I. Mondragon and J. Labidi, *Chem. Eng. J.*, 2010, **157**, 93–99.
63 J. W. Collins, J. M. Torkelson and A. A. Webb, *J. Agric. Food Chem.*, 1977, **25**, 743–746.
64 M. Norgren and B. Lindström, 2000, **54**, pp. 528–534.
65 O. Sevastyanova, M. Helander, S. Chowdhury, H. Lange, H. Wedin, L. Zhang, M. Ek, J. F. Kadla, C. Crestini and M. E. Lindström, *J. Appl. Polym. Sci.*, 2014, **131**, DOI: **10.1002/app.40799**.
66 A. Keyoumu, R. Sjödahl, G. Henriksson, M. Ek, G. Gellerstedt and M. E. Lindström, *Ind. Crops Prod.*, 2004, **20**, 143–150.
67 C. A. E. Costa, P. C. R. Pinto and A. E. Rodrigues, *Sep. Purif. Technol.*, 2018, **192**, 140–151.
68 C. Allegretti, S. Fontanay, Y. Krauke, M. Luebbert, A. Strini, J. Troquet, S. Turri, G. Griffini and P. D'Arrigo, *ACS SustainableChem. Eng.*, 2018, **6**, 9056–9064.
69 A. Aher, R. Sarma, M. Crocker and D. Bhattacharyya, *Sep. Purif. Technol.*, 2020, **230**, 115865.
70 R. E. Majdar, C. Crestini and H. Lange, *ChemSusChem*, 2020, **13**, 4735–4742.
71 C. Crestini, H. Lange and D. Argyropoulos, *WO Pat.*, WO2020128034A1, World Intellectual Property Organization, 2020.
72 N. Pajer, C. Cestari, D. S. Argyropoulos and C. Crestini, *npj Mater. Sustain.*, 2024, **2**, 1–9.
73 C. Cestari, N. Pajer and C. Crestini, in *Reference Module in Chemistry, Molecular Sciences and Chemical Engineering*, Elsevier, 2024.
74 D. S. Argyropoulos and C. Crestini, *ACS Sustainable Chem. Eng.*, 2016, **4**, 5089.
75 N. Pajer, M. Gigli and C. Crestini, *ChemSusChem*, 2024, **17**, e202301646.
76 R. M. Ede, J. Ralph, K. M. Torr and B. Watson, 1996, **50**, pp. 161–164.

77 G. Brunow and K. Lundquist, in *Lignin and Lignans. Advances in Chemistry*, CRC Press, Boca Raton, 1st edn, 2010, pp. 267–300.
78 R. H. J. Creighton and H. Hibbert, *J. Am. Chem. Soc.*, 1944, **66**, 37–38.
79 R. H. J. Creighton, R. D. Gibbs and H. Hibbert, *J. Am. Chem. Soc.*, 1944, **66**, 32–37.
80 T. Higuchi, Y. Ito, M. Shimada and I. Kawamura, *Phytochemistry*, 1967, **6**, 1551–1556.
81 K. Freudenberg, *Pure Appl. Chem.*, 1962, **5**, 9–20.
82 C. Crestini, F. Melone, M. Sette and R. Saladino, *Biomacromolecules*, 2011, **12**, 3928–3935.
83 C. Crestini, H. Lange, M. Sette and D. S. Argyropoulos, *Green Chem.*, 2017, **19**, 4104–4121.
84 A. Guerra, I. Filpponen, L. A. Lucia, C. Saquing, S. Baumberger and D. S. Argyropoulos, *J. Agric. Food Chem.*, 2006, **54**, 5939–5947.
85 A. Guerra, I. Filpponen, L. A. Lucia and D. S. Argyropoulos, *J. Agric. Food Chem.*, 2006, **54**, 9696–9705.
86 A. Granata and D. S. Argyropoulos, *J. Agric. Food Chem.*, 1995, **43**, 1538–1544.
87 X. Meng, C. Crestini, H. Ben, N. Hao, Y. Pu, A. J. Ragauskas and D. S. Argyropoulos, *Nat. Protoc.*, 2019, **14**, 2627–2647.
88 D. S. Argyropoulos, N. Pajer and C. Crestini, *J. Visualized Exp.*, 2021, 62696.
89 M. Ragnar, C. T. Lindgren and N.-O. Nilvebrant, *J. Wood Chem. Technol.*, 2000, **20**, 277–305.
90 M. Österberg, K. A. Henn, M. Farooq and J. J. Valle-Delgado, *Chem. Rev.*, 2023, **123**, 2200–2241.
91 M. Lievonen, J. J. Valle-Delgado, M.-L. Mattinen, E.-L. Hult, K. Lintinen, M. A. Kostiainen, A. Paananen, G. R. Szilvay, H. Setälä and M. Österberg, *Green Chem.*, 2016, **18**, 1416–1422.
92 L. Zongo, H. Lange and C. Crestini, *ACS Omega*, 2019, **4**, 6979–6993.
93 J. V. Vermaas, M. F. Crowley and G. T. Beckham, *ACS Sustainable Chem. Eng.*, 2020, **8**, 17839–17850.
94 W. Zhao, B. Simmons, S. Singh, A. Ragauskas and G. Cheng, *Green Chem.*, 2016, **18**, 5693–5700.
95 M. Gigli, S. Cailotto and C. Crestini, in *Biorefinery: from Biomass to Chemicals and Fuels*, De Gruyter, 2021, pp. 265–320.
96 M. H. Sipponen, H. Lange, C. Crestini, A. Henn and M. Österberg, *ChemSusChem*, 2019, **12**, 2039–2054.
97 A. Boarino and H.-A. Klok, *Biomacromolecules*, 2023, **24**, 1065–1077.
98 S. R. Yearla and K. Padmasree, *J. Exp. Nanosci.*, 2016, **11**, 289–302.
99 H. Sadeghifar and A. Ragauskas, *Polymers*, 2020, **12**, 1134.
100 F. Lu and J. Ralph, *J. Agric. Food Chem.*, 1998, **46**, 547–552.
101 E. Adler, J. M. Pepper and E. Eriksoo, *Ind. Eng. Chem.*, 1957, **49**, 1391–1392.
102 C. Rolando, B. Monties and C. Lapierre, in *Methods in Lignin Chemistry*, ed. S. Y. Lin and C. W. Dence, Springer, Berlin, Heidelberg, 1992, pp. 334–349.
103 E. Adler and K. Lundquist, *Acta Chem. Scand.*, 1963, **17**, 13–26.
104 K. Lundquist, in *Methods in Lignin Chemistry*, ed. S. Y. Lin and C. W. Dence, Springer, Berlin, Heidelberg, 1992, pp. 289–300.
105 G. Brunow, I. Kilpeläinen, J. Sipilä, K. Syrjänen, P. Karhunen, H. Setälä and P. Rummakko, in *Lignin and Lignan Biosynthesis*, American Chemical Society, 1998, vol. 697, pp. 131–147.

106 P. Karhunen, P. Rummakko, J. Sipilä, G. Brunow and I. Kilpeläinen, *Tetrahedron Lett.*, 1995, **36**, 169–170.
107 K. Freudenberg and K.-C. Renner, *Chem. Ber.*, 1965, **98**, 1879–1892.
108 K. Kratzl, J. Gratzl and P. Claus, in *Lignin Structure and Reactions*, American Chemical Society, 1966, vol. 59, pp. 157–176.
109 J. Gierer, *Wood Sci. Technol.*, 1980, **14**, 241–266.
110 J. Gierer, *Wood Sci. Technol.*, 1986, **20**, 1–33.
111 J. Gierer, *Wood Sci. Technol.*, 1985, **19**, 289–312.
112 J. Gierer, *Journal of Wood Science and Technology*, 1982, **36**, 55–64.
113 J. S. Gratzl and C.-L. Chen, in *Lignin: Historical, Biological, and Materials Perspectives*, American Chemical Society, 1999, vol. 742, pp. 392–421.
114 M. Karlsson, J. Romson, T. Elder, Å. Emmer and M. Lawoko, *Biomacromolecules*, 2023, **24**, 2314–2326.
115 O. Musl, I. Sulaeva, I. Sumerskii, A. K. Mahler, T. Rosenau, J. Falkenhagen and A. Potthast, *ACS Sustainable Chem. Eng.*, 2021, **9**, 16786–16795.
116 A. More, T. Elder, N. Pajer, D. S. Argyropoulos and Z. Jiang, *ACS Omega*, 2023, **8**, 1097–1108.
117 M. B. Peralta, N. Pajer, C. Crestini and V. V. Nicolau, *Wood Sci. Technol.*, 2024, **58**, 2047–2072.
118 C. Nitsos, R. Stoklosa, A. Karnaouri, D. Vörös, H. Lange, D. Hodge, C. Crestini, U. Rova and P. Christakopoulos, *ACS Sustainable Chem. Eng.*, 2016, **4**, 5181–5193.
119 P. Jõul, T. T. Ho, U. Kallavus, A. Konist, K. Leiman, O.-S. Salm, M. Kulp, M. Koel and T. Lukk, *Materials*, 2022, **15**, 2861.
120 R. Sheibani, H. Gharoubi, A. Parandoust, M. Sheibani, N. Pajer and D. S. Argyropoulos, *Inorg. Chem. Commun.*, 2023, **156**, 111200.
121 P. K. Mishra and A. Ekielski, *Nanomaterials*, 2019, **9**, 243.
122 T. Lindström, *Colloid Polym. Sci.*, 1979, **257**, 277–285.
123 M. Kasha, H. R. Rawls and M. Ashraf El-Bayoumi, *Pure Appl. Chem.*, 1965, **11**, 371–392.
124 D. R. Ratnaweera, D. Saha, S. V. Pingali, N. Labbé, A. K. Naskar and M. Dadmun, *RSC Adv.*, 2015, **5**, 67258–67266.
125 A. Dastpak, T. V. Lourençon, M. Balakshin, S. Farhan Hashmi, M. Lundström and B. P. Wilson, *Ind. Crops Prod.*, 2020, **148**, 112310.
126 C. Schuerch, *J. Am. Chem. Soc.*, 1952, **74**, 5061–5067.
127 J. Koleske and C. Hansen, *Chapter 35 – Paint and Coating Testing Manual, Fourteenth Edition of the Gardner-Sward Handbook*, 2009.
128 M. H. Sipponen, H. Lange, M. Ago and C. Crestini, *ACS Sustainable Chem. Eng.*, 2018, **6**, 9342–9351.
129 I. V. Pylypchuk, M. Karlsson, P. A. Lindén, M. E. Lindström, T. Elder, O. Sevastyanova and M. Lawoko, *Green Chem.*, 2023, **25**, 4415–4428.
130 A. Duval, F. Vilaplana, C. Crestini and M. Lawoko, *Holzforschung*, 2016, **70**, 11–20.
131 K. Freudenberg and W. Lautsch, *Naturwissenschaften*, 1939, **27**, 227–228.
132 J. D. Zwilling, X. Jiang, F. Zambrano, R. A. Venditti, H. Jameel, O. D. Velev, O. J. Rojas and R. Gonzalez, *Green Chem.*, 2021, **23**, 1001–1012.
133 Q. Li, H. Zhang, J. Lee and C. Wan, *Green Chem.*, 2023, **25**, 9301–9312.
134 A. Myerson, D. Erdemir and A. Y. Lee, *Handbook of Industrial Crystallization. Cambridge University Pre*, Cambridge University Press, Cambridge, USA, 2019.

135 N. T. K. Thanh, N. Maclean and S. Mahiddine, *Chem. Rev.*, 2014, **114**, 7610–7630.
136 X. Zhang, J. Zhang, H. Yang, C. He, Y. Ke, S. Singh and G. Cheng, *ChemSusChem*, 2022, **15**, e202201230.
137 M. Yang, W. Zhao, S. Singh, B. Simmons and G. Cheng, *Nanoscale Adv.*, 2019, **1**, 299–304.
138 I. V. Pylypchuk, A. Riazanova, M. E. Lindström and O. Sevastyanova, *Green Chem.*, 2021, **23**, 3061–3072.
139 L. Chen, S.-M. Luo, C.-M. Huo, Y.-F. Shi, J. Feng, J.-Y. Zhu, W. Xue and X. Qiu, *Green Chem.*, 2022, **24**, 285–294.
140 S. Beisl, A. Miltner and A. Friedl, *Int. J. Mol. Sci.*, 2017, **18**, 1244.
141 S. Iravani and R. S. Varma, *Green Chem.*, 2020, **22**, 612–636.
142 S. Salentinig and M. Schubert, *Biomacromolecules*, 2017, **18**, 2649–2653.
143 F. Xiong, Y. Han, S. Wang, G. Li, T. Qin, Y. Chen and F. Chu, *Ind. Crops Prod.*, 2017, **100**, 146–152.
144 I. V. Pylypchuk, P. A. Lindén, M. E. Lindström and O. Sevastyanova, *ACS Sustainable Chem. Eng.*, 2020, **8**, 13805–13812.
145 W. Zhao, L.-P. Xiao, G. Song, R.-C. Sun, L. He, S. Singh, B. A. Simmons and G. Cheng, *Green Chem.*, 2017, **19**, 3272–3281.
146 G. Hu, J. Hu, H. Chen, S. Song and F. Chu, *Bioresearch*, 2021, **16**, 7608–7622.
147 N. Alipoormazandarani, T. Benselfelt, L. Wang, X. Wang, C. Xu, L. Wågberg, S. Willför and P. Fatehi, *ACS Appl. Mater. Interfaces*, 2021, **13**(22), 26308–26317.
148 K. D. Collins, *Biophys. J.*, 1997, **72**, 65–76.
149 T. Leskinen, M. Smyth, Y. Xiao, K. Lintinen, M.-L. Mattinen, M. A. Kostiainen, P. Oinas and M. Österberg, *Nordic Pulp Paper Res. J.*, 2017, **32**(4), 586–596.
150 M. Norgren, H. Edlund and L. Wågberg, *Langmuir*, 2002, **18**, 2859–2865.
151 H. Chum, *Assessment of Biobased Materials*, 1989.
152 M. Ago, B. L. Tardy, L. Wang, J. Guo, A. Khakalo and O. J. Rojas, *MRS Bull.*, 2017, **42**, 371–378.
153 M. Österberg, M. H. Sipponen, B. D. Mattos and O. J. Rojas, *Green Chem.*, 2020, **22**, 2712–2733.
154 M. A. Hubbe, R. Trovagunta, F. Zambrano, P. Tiller and J. Jardim, *BioResources*, 2023, **18**, 4262–4331.
155 D. Yiamsawas, G. Baier, E. Thines, K. Landfester and F. R. Wurm, *RSC Adv.*, 2014, **4**, 11661–11663.
156 Y. Qian, Y. Deng, X. Qiu, H. Li and D. Yang, *Green Chem.*, 2014, **16**, 2156–2163.
157 T. Li, S. Lü, Z. Wang, M. Huang, J. Yan and M. Liu, *Sci. Total Environ.*, 2021, **765**, 142745.
158 C. Li, Q. Ping, H. Shi, N. Li, J. Zhang and C. Wang, *Int. J. Biol. Macromol.*, 2019, **156**, 1483–1490.
159 J. Yu, L. Li, Y. Qian, H. Lou, D. Yang and X. Qiu, *Ind. Eng. Chem. Res.*, 2018, **57**, 15740–15748.
160 W. Yang, E. Fortunati, F. Dominici, G. Giovanale, A. Mazzaglia, G. M. Balestra, J. M. Kenny and D. Puglia, *Eur. Polym. J.*, 2016, **79**, 1–12.
161 X. He, F. Luzi, X. Hao, W. Yang, L. Torre, Z. Xiao, Y. Xie and D. Puglia, *Int. J. Biol. Macromol.*, 2019, **127**, 665–676.
162 S. R. Yearla and K. and Padmasree, *J. Exp. Nanosci.*, 2016, **11**, 289–302.

163 E. D. Bartzoka, H. Lange, K. Thiel and C. Crestini, *ACS Sustainable Chem. Eng.*, 2016, **4**, 5194–5203.
164 M. Tortora, F. Cavalieri, P. Mosesso, F. Ciaffardini, F. Melone and C. Crestini, *Biomacromolecules*, 2014, **15**, 1634–1643.
165 A. A. Myint, H. W. Lee, B. Seo, W.-S. Son, J. Yoon, T. J. Yoon, H. J. Park, J. Yu, J. Yoon and Y.-W. Lee, *Green Chem.*, 2016, **18**, 2129–2146.
166 Y. Li, X. Qiu, Y. Qian, W. Xiong and D. Yang, *Chem. Eng. J.*, 2017, **327**, 1176–1183.
167 P. Figueiredo, K. Lintinen, A. Kiriazis, V. Hynninen, Z. Liu, T. Bauleth-Ramos, A. Rahikkala, A. Correia, T. Kohout, B. Sarmento, J. Yli-Kauhaluoma, J. Hirvonen, O. Ikkala, M. A. Kostiainen and H. A. Santos, *Biomaterials*, 2017, **121**, 97–108.
168 H. Sadeghifar and D. S. Argyropoulos, *ACS Sustainable Chem. Eng.*, 2015, **3**, 349–356.
169 H. Sadeghifar and D. S. Argyropoulos, *ACS Sustainable Chem. Eng.*, 2016, **4**, 5160–5166.
170 P. Alexy, B. Košíková and G. Podstránska, *Polymer*, 2000, **41**, 4901–4908.
171 D. S. Argyropoulos, R. M. Berry and H. I. Bolker, *Die Makromolekulare Chem.*, 1987, **188**, 1985–1992.
172 P. J. Flory, *J. Am. Chem. Soc.*, 1941, **63**, 3083–3090.
173 W. H. Stockmayer, *J. Chem. Phys.*, 1944, **12**, 125–131.
174 D. Dong and A. L. Fricke, *Polymer*, 1995, **36**, 2075–2078.
175 A. Guerra, A. R. Gaspar, S. Contreras, L. A. Lucia, C. Crestini and D. S. Argyropoulos, *Phytochemistry*, 2007, **68**, 2570–2583.
176 S. Contreras, A. R. Gaspar, A. Guerra, L. A. Lucia and D. S. Argyropoulos, *Biomacromolecules*, 2008, **9**, 3362–3369.
177 G. Toriz, F. Denes and R. A. Young, *Polym. Compos.*, 2002, **23**, 806–813.
178 C. González Sánchez and L. A. E. Alvarez, *Die Angewandte Makromolekulare Chemie*, 1999, **272**, 65–70.
179 S. Sen, H. Sadeghifar and D. S. Argyropoulos, *Biomacromolecules*, 2013, **14**, 3399–3408.
180 W. J. Sagues, A. Jain, D. Brown, S. Aggarwal, A. Suarez, M. Kollman, S. Park and D. S. Argyropoulos, *Green Chem.*, 2019, **21**, 4253–4265.
181 M. Al Aiti, D. Jehnichen, D. Fischer, H. Brünig and G. Heinrich, *Prog. Mater. Sci.*, 2018, **98**, 477–551.
182 E. Fitzer and L. M. Manocha, *Carbon Reinforcements and Carbon/Carbon Composites*, Springer, Berlin, Heidelberg, 1998.
183 A. Galiguzov, A. Malakho, V. Kulakov, A. Kenigfest, E. Kramarenko and V. Avdeev, *Carbon Lett.*, 2013, **14**, 22–26.
184 A. P. Nowak, J. Hagberg, S. Leijonmarck, H. Schweinebarth, D. Baker, A. Uhlin, P. Tomani and G. Lindbergh, *Holzforschung*, 2018, **72**, 81–90.
185 M. S. Kim, D. H. Lee, C. H. Kim, Y. J. Lee, J. Y. Hwang, C.-M. Yang, Y. A. Kim and K. S. Yang, *Carbon*, 2015, **85**, 194–200.
186 L. M. Steudle, E. Frank, A. Ota, U. Hageroth, S. Henzler, W. Schuler, R. Neupert and M. R. Buchmeiser, *Macromol. Mater. Eng.*, 2017, **302**, 1600441.
187 A. A. Ogale, M. Zhang and J. Jin, *J. Appl. Polym. Sci.*, 2016, **133**, DOI: **10.1002/app.43794**.
188 Q. Li, S. Xie, W. K. Serem, M. T. Naik, L. Liu and J. S. Yuan, *Green Chem.*, 2017, **19**, 1628–1634.

189 R. E. Franklin and J. T. Randall, *Proc. R. Soc. A*, 1997, **209**, 196–218.
190 M. S. A. Rahaman, A. F. Ismail and A. Mustafa, *Polym. Degrad. Stab.*, 2007, **92**, 1421–1432.
191 M. Foston, G. A. Nunnery, X. Meng, Q. Sun, F. S. Baker and A. Ragauskas, *Carbon*, 2013, **52**, 65–73.
192 Q. Sun, R. Khunsupat, K. Akato, J. Tao, N. Labbé, N. C. Gallego, J. J. Bozell, T. G. Rials, G. A. Tuskan, T. J. Tschaplinski, A. K. Naskar, Y. Pu and A. J. Ragauskas, *Green Chem.*, 2016, **18**, 5015–5024.
193 F. Souto, V. Calado and N. Pereira, *Mater. Res. Express*, 2018, **5**, 072001.
194 X. Zhang, Q. Yan, W. Leng, J. Li, J. Zhang, Z. Cai and E. B. Hassan, *Materials*, 2017, **10**, 975.
195 H. Sadeghifar, S. Sen, S. V. Patil and D. S. Argyropoulos, *ACS Sustainable Chem. Eng.*, 2016, **4**, 5230–5237.
196 D. A. Baker and T. G. Rials, *J. Appl. Polym. Sci.*, 2013, **130**, 713–728.
197 F. S. Baker, *Low Cost Carbon Fiber From Renewable Resources*, 2010, **https://https://www1.eere.energy.gov/vehiclesandfuels/pdfs/merit_review_2010/lightweight_materials/lm005_baker_2010_o.pdf**, accessed 10/09/2025.
198 A. P. Nowak, J. Hagberg, S. Leijonmarck, H. Schweinebarth, D. Baker, A. Uhlin, P. Tomani and G. Lindbergh, *Holzforschung*, 2018, **72**, 81–90.
199 W. E. Tenhaeff, O. Rios, K. More and M. A. McGuire, *Adv. Funct. Mater.*, 2014, **24**, 86–94.
200 J. Köhnke, H. Rennhofer, H. Lichtenegger, A. raj Mahendran, C. Unterweger, B. Prats-Mateu, N. Gierlinger, E. Schwaiger, A.-K. Mahler, A. Potthast and W. Gindl-Altmutter, *ACS Sustainable Chem. Eng.*, 2018, **6**, 3385–3391.
201 J. Jin, J. Ding, A. Klett, M. C. Thies and A. A. Ogale, *ACS Sustainable Chem. Eng.*, 2018, **6**, 14135–14142.
202 H. Liu, Z. Dai, Q. Cao, X. Shi, X. Wang, H. Li, Y. Han, Y. Li and J. Zhou, *ACS Sustainable Chem. Eng.*, 2018, **6**, 8554–8562.
203 E. Frank, F. Hermanutz and M. R. Buchmeiser, *Macromol. Mater. Eng.*, 2012, **297**, 493–501.
204 D. A. Baker, N. C. Gallego and F. S. Baker, *J. Appl. Polym. Sci.*, 2012, **124**, 227–234.
205 S. Kubo, Y. Uraki and Y. Sano, *J. Wood Sci.*, 2003, **49**, 188–192.
206 A. Gomez-Martin, J. Martinez-Fernandez, M. Ruttert, A. Heckmann, M. Winter, T. Placke and J. Ramirez-Rico, *ChemSusChem*, 2018, **11**, 2776–2787.
207 X. Xu, J. Zhou, L. Jiang, G. Lubineau, S. A. Payne and D. Gutschmidt, *Carbon*, 2014, **80**, 91–102.
208 S. A. I. Steiner, R. Li and B. L. Wardle, *ACS Appl. Mater. Interfaces*, 2013, **5**, 4892–4903.
209 K. J. Kim, J. Kim, W.-R. Yu, J. H. Youk and J. Lee, *Carbon*, 2013, **54**, 258–267.
210 F. J. García-Mateos, T. Cordero-Lanzac, R. Berenguer, E. Morallón, D. Cazorla-Amorós, J. Rodríguez-Mirasol and T. Cordero, *Appl. Catal., B*, 2017, **211**, 18–30.